MULTISCALE MODEL. SIMUL.
Vol. 15, No. 2, pp. 920–947

OPTIMIZATION OF FIRST PASSAGE TIMES BY MULTIPLE COOPERATING MOBILE TRAPS*

A. E. LINDSAY†, J. C. TZOU‡, AND T. KOLOKOLNIKOV§

Abstract. We study the mean capture time of an unbiased random walker by multiple absorbing mobile traps in bounded domains of one and two spatial dimensions. In one dimension, we consider multiple traps undergoing prescribed oscillatory motion on an interval with reflecting or absorbing boundary conditions. We develop trap cooperation strategies which optimize the mean capture time. We find that as the frequency of oscillation passes through certain fixed values, the optimal trap strategy alternates between oscillating exactly in phase and exactly out of phase with neighboring traps. We also demonstrate a scenario in which the optimal configuration is neither in phase nor antiphase. In two dimensions, we consider two small traps rotating with the same angular velocity ω inside a unit disk and characterize the optimal positions (radii of rotation and relative phase) of the two traps as a function of ω and trap radius $\varepsilon \ll 1$. We identify several distinguished regimes in ω where the optimal configuration can be distinctly characterized. In particular, in the $\omega \sim \mathcal{O}(1)$ regime, the optimal configuration jumps from one in which two traps rotate antipodal and along the same radius to one where the two traps rotate on the same side of the disk but at different radii. In addition, we demonstrate an algebraic approach to obtaining optimal configurations of N rotating traps as $\omega \to \infty$.

Key words. mean first passage time, multiple mobile traps, trap cooperation, asymptotic analysis, optimization strategy

AMS subject classifications. 35B25, 35C20, 35J05, 35J08

DOI. 10.1137/16M1060169

1. Introduction.

We study the problem for the mean first passage time (MFPT) of a randomly diffusing particle to multiple absorbing mobile traps which undertake a prescribed motion in bounded regions of one and two spatial dimensions. Random motion is a ubiquitous transport mechanism in many biological, physical, and chemical systems. Often, a significant event is triggered when a dispersing particle reaches a particular site or meets another particle. Consequently, many important processes may be formulated as an MFPT problem for the expected time taken for a particle to hit a trap. One-dimensional examples arise in finance, where an investor sells a stock when it reaches a certain threshold, and in sequential analysis and goodness of fit tests in statistics [11].

In two and three dimensions, a special case known as a *narrow escape* or *narrow capture problem* (see, e.g., [26, 27, 28, 21, 8, 23, 2]) arises when the size of the trap is small in comparison to that of the search domain. For example, intracellular processes require proteins to diffuse in the cytoplasm until they reach the nucleus, where they are transported to the interior through nuclear pore complexes distributed on its surface

*Received by the editors February 5, 2016; accepted for publication (in revised form) February 8, 2017; published electronically June 7, 2017.

http://www.siam.org/journals/mms/15-2/M106016.html

Funding: The first author was supported by NSF grant DMS-1516753. The second author was supported by a PIMS CRG fellowship. The third author was supported by NSERC Discovery Grant RGPIN-33798 and NSERC Accelerator Grant RGPAS/461907.

†Department of Applied and Computational Mathematics and Statistics, University of Notre Dame, Notre Dame, IN 46556 (a.lindsay@nd.edu).

‡Mathematics Department, University of British Columbia, Vancouver, BC, V6T 1Z2, Canada (tzou.justin@gmail.com).

§Department of Mathematics and Statistics, Dalhousie University, Halifax, NS, B3H 3J5, Canada (tkolokol@gmail.com).

[22, 16, 14, 13]. The cell nucleus is modeled as a small interior trap as its volume is small in comparison to that of the whole cell. Conversely, when ions diffuse in search of an open ion channel located on the cell membrane [6, 23, 26, 18], the traps may be modeled as small absorbing portions of an otherwise reflective boundary. The search for antigen presenting molecules in lymph node tissue by T cells may be modeled as a three-dimensional narrow escape problem with interior traps [12] in which MFPT yields insight into immune system recognition. The applications of narrow escape problems are numerous, and we refer to [20, 19, 7] for detailed reviews.

Existing mathematical treatments of these examples predominantly assume that traps occupy a fixed location over time. However, in many applications traps are known to be mobile. In the example of intracellular transport, the cell nucleus is in motion before and after mitosis [29]; therefore proteins must diffuse to mobile targets in order to complete their processes. In one dimension, a scenario lending to mobile targets is that of fixation times in population genetics (see [31] and references therein). In this work, we investigate mean survival times of random walkers in the presence of multiple traps undergoing prescribed motion along a constrained path. In particular, we study the question of how multiple mobile searchers should cooperate in order to most quickly locate a diffusing target. We cite as a typical scenario the search for a lost person by a team of rescuers.

MFPT problems involving mobile traps have been gaining attention for their various applications and also because there is not yet a systematic methodology for their analysis as exists for stationary traps. A recent review on MFPT problems in bounded domains [3] cited the generalization to mobile traps as an interesting extension. Many works in this new direction have focused on one-dimensional problems, where the mobile trap either undergoes random motion or advances in one direction linearly in time [10, 5, 4, 15, 17, 30].

An overarching question is whether a mobile trap is more or less effective than a stationary one. In [33], it was shown that a single trap undergoing sinusoidal motion in a bounded one-dimensional interval is more effective only when the frequency exceeds a certain threshold. This criticality can be heuristically understood from a balance between two competing factors that contribute to the MFPT. First, the placement of the absorbing trap at the center of the one-dimensional interval results in a lower MFPT. Second, trap mobility allows a trap to explore its space more effectively and so improves its trapping ability. Therefore, a mobile trap is superior to a stationary one only when it moves quickly enough to overcome the detrimental effects of moving away from optimal spatial locations.

A similar two-dimensional result was established in [32] for a single trap rotating inside the unit disk. The presence of two variables of motion (frequency and radius of rotation) poses a simple optimization problem: for a given frequency, what is the radius of rotation that would minimize average MFPT? In this setting, a similar criticality is observed where the trap must rotate sufficiently quickly to offset the detrimental effect of moving off the origin—the optimal spatial location for the unit disk [21].

In the present work, we analyze MFPT problems in bounded one- and two-dimensional regions with *multiple* mobile traps with prescribed trajectories and emphasize the optimization of average (or global) MFPT with respect to the relative motion between the traps. In section 2, we consider a diffusing particle on a one-dimensional interval with reflecting or absorbing end points and absorbing internal traps with small amplitude oscillations ε at common frequency ω and centered on fixed points with separation ℓ. A schematic of the one-dimensional two-trap problem

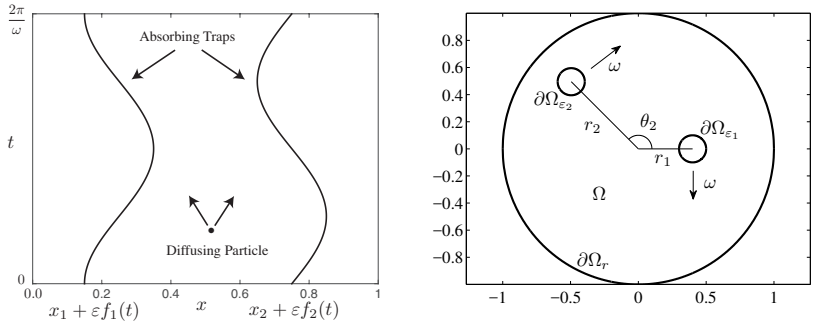

(a) Schematic of 1D problem. (b) Schematic of 2D problem.

FIG. 1. (a) *A schematic of the one-dimensional problem with two traps. Two traps oscillate in time at the same frequency tracing out the paths indicated by the curves. Their relative phase is arbitrary.* (b) *A schematic of the two-dimensional problem with two traps. In the reference frame rotating clockwise at frequency ω, the first trap is placed on the horizontal axis (without loss of generality) at a distance r_1 from the origin. The second trap is phase shifted counterclockwise by angle θ_2 and is a distance r_2 from the origin. Both traps have common radius ε.*

is displayed in Figure 1(a). The linearity of the governing equations allows for trivial extension of the present work to trap trajectories with multiple frequency components. However, we focus herein on trajectories described by a single frequency component as the resulting motion minimizes the MFPT under a fixed kinetic energy constraint.

We show in the one-dimensional setup of Figure 1(a) that the mean capture time of the particle averaged uniformly over all starting locations (often referred to as global MFPT) is minimized when the two traps oscillate either exactly in phase or exactly antiphase, depending on the sign a certain quantity $\chi(\omega\ell^2)$, where

$$\chi(z) = \left[\frac{\cosh\sqrt{\frac{z}{2}}\sin\sqrt{\frac{z}{2}} + \sinh\sqrt{\frac{z}{2}}\cos\sqrt{\frac{z}{2}}}{\cos\sqrt{2z} - \cosh\sqrt{2z}} \right],$$

the trap separation as $\varepsilon \to 0$ is ℓ, and the common frequency is ω. The oscillatory nature of $\chi(z)$ means that the optimal strategy alternates as the frequency of the trap's motion increases. In section 2.1, these results are extended to N traps oscillating about fixed points x_j with small amplitude ε and common frequency ω. We determine that the globally optimal cooperation strategy corresponds to neighboring traps oscillating either exactly in phase or exactly out of phase depending on the sign of $\chi(\omega\ell_j^2)$, where $\ell_j = x_{j+1} - x_j$. However, in the scenario where a new trap is inserted between two existing traps whose trajectories are fixed, the optimal strategy of the new trap is not necessarily in or out of phase with its neighbors.

In section 3, we consider N small traps of radius $0 < \varepsilon \ll 1$ rotating clockwise with common frequency ω at distances r_j from the center of a unit disk with $j = 1, \ldots, N$ (schematic in Figure 1(b)). We use a matched asymptotics approach (e.g., [32, 21, 23]) to compute the global MFPT of a randomly diffusing particle. Our formulation allows for arbitrary phase differences between the traps. For $N = 2$, we perform a numerical optimization of the global MFPT with respect to the two radii of rotation in addition to the relative phase. The results of optimization show that as ω increases past a critical $\mathcal{O}(1)$ frequency, the optimal configuration of the traps switches from rotating at the same radius but π-radians out of phase to rotating at different

radii but exactly in phase. We also show that in the regime $\mathcal{O}(1) \ll \omega \ll \mathcal{O}(\varepsilon^{-1})$, the optimal radii of N traps divides the unit disk into N annuli of equal area (with the outermost radius approaching the boundary). We also derive an analogous result in the regime $\omega \gg \mathcal{O}(\varepsilon^{-1})$. We further use a hybrid numeric-asymptotic method [9, 32] to interpolate between these two regimes, showing that the transition between the regimes is smooth. In section 4, we draw conclusions and list open avenues for further work.

2. Multiple traps in one dimension. In this section we consider the MFPT problem in a bounded one-dimensional interval with reflecting stationary end points and two mobile internal traps undergoing prescribed oscillatory motion with period $2\pi/\omega$. The main idea in the formulation of these moving domain problems is to project the trap motion in a new direction, orthogonal to the walker's spatial motion, and coupled to an advection term in that direction (cf. Figure 2).

For a random walk with Brownian dynamics in the x direction and deterministic transport in the positive t direction, the equation satisfied by the MFPT $u(x,t)$ of a particle initially at (x,t) is derived by first considering discrete jumps of size Δx in the time interval $(t, t+\Delta t)$. This yields that

$$u(x,t) = \Delta t + \frac{1}{2}\Big[u(x+\Delta x, t+\Delta t) + u(x-\Delta x, t+\Delta t)\Big]. \tag{2.1}$$

In the limit $\Delta x \to 0$ and $\Delta t \to 0$ with $D = \Delta x^2/(2\Delta t)$ fixed, (2.1) reduces to the partial differential equation [5, 25, 33]

(2.2a)

$$u_t + Du_{xx} + 1 = 0; \quad 0 < x < 1; \quad 0 < t < \frac{2\pi}{\omega}; \qquad u(x,0) = u\left(x, \frac{2\pi}{\omega}\right), \quad 0 < x < 1,$$

for the MFPT $u(x,t)$, starting from (x,t). This approach is readily applicable to nonstationary boundaries with a variety of boundary conditions. In what follows, we consider the boundary conditions

$$u_x(0,t) = u_x(1,t) = 0, \tag{2.2b}$$

$$u(x_1 + \varepsilon f_1(t)) = u(x_2 + \varepsilon f_2(t)) = 0, \tag{2.2c}$$

so that the domain exterior is reflecting and there are two absorbing interior traps. For convenience, the diffusivity will be normalized to one for the remainder of the treatment. Each mode in the dynamics of a trap can be considered in isolation due to the linearity of (2.1), so the two absorbing traps (2.2c) are assumed to undergo motion

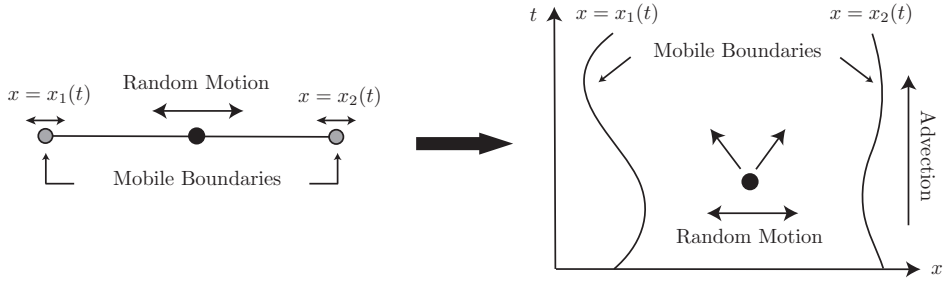

FIG. 2. *Schematic of transforming the moving one-dimensional problem to a static two-dimensional problem.*

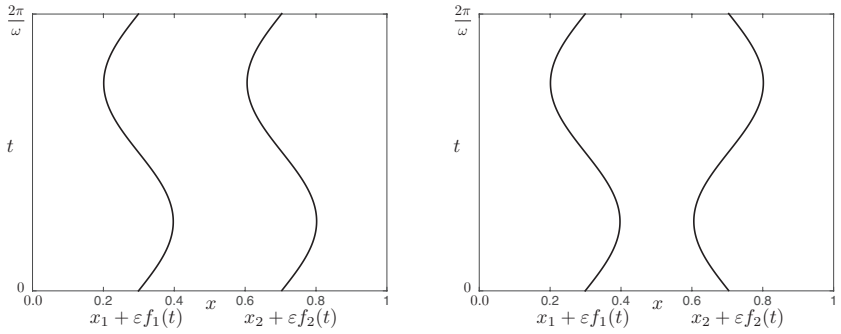

(a) In phase: $\phi = 0$. (b) Out of phase: $\omega\phi = \pi$.

FIG. 3. *The in-phase (left panel $\phi = 0$) and out-of-phase (right panel $\omega\phi = \pi$) cooperation strategies for two mobile traps. Plotted for $x_1 = 0.3, x_2 = 0.7$, and $\varepsilon = 0.1$.*

with a common frequency ω, but with a phase shift according to their cooperation strategy,

$$f_1(t) = \sin \omega t, \qquad f_2(t) = \sin \omega(t - \phi), \qquad \phi \in \left(0, \frac{2\pi}{\omega}\right). \tag{2.2d}$$

In Figure 3, the two extremal cooperation strategies are displayed with $\phi = 0$ and $\phi = \pi/\omega$ indicating in and out of phase cooperation strategies, respectively. The main goal is to understand how the relative motion of the traps affects the mean time to capture. In particular, for which values of ϕ is the MFPT optimized? To study this we calculate the global MFPT

$$\tau(\omega; \phi) = \frac{\omega}{2\pi} \int_0^{\frac{2\pi}{\omega}} \int_{x=0}^{1} u(x,t)\, dx dt\,, \tag{2.3}$$

which gives a measure of the trapping effectiveness of the configuration. From this quantity, optimizing configurations of ϕ and ω can be determined. In the limit $\varepsilon \to 0$, (2.2) admits a regular expansion of form

$$u(x,t) = u_0(x) + \varepsilon u_1(x,t) + \varepsilon^2 u_2(x,t) + \mathcal{O}\left(\varepsilon^3\right), \tag{2.4a}$$

with $u_x(0,t) = u_x(1,t) = 0$. Expanding around the trapping boundaries supplements the equations with the internal conditions

(2.4b)
$$u_0(x_j) = 0, \quad u_1(x_j) = -u_0'(x_j) f_1, \quad u_2(x_j) = -\frac{u_0''(x_j)}{2} f_1^2 - u_1'(x_j) f_1, \quad j = 1, 2.$$

This subdivides the interval $\Omega = [0, 1]$ into three distinct regions:

(2.4c)
$$\mathcal{R}_1(t) = (0, x_1 + \varepsilon f_1(t)), \quad \mathcal{R}_2(t) = (x_1 + \varepsilon f_1(t), x_2 + \varepsilon f_2(t)), \quad \mathcal{R}_3(t) = (x_2 + \varepsilon f_2(t), 1).$$

In the analysis that follows, the regular expansion (2.4a) is substituted into equation (2.2) and terms gathered at each order of ε. This generates a sequence of reduced

problems for $u_0, u_1, u_2, \ldots$ for which explicit solutions satisfying boundary conditions (2.4b) are obtained. From these solutions, the global MFPT arising from a uniform distribution of initial locations can be obtained by explicit integration of τ defined in (2.3). Once this explicit expression for $\tau(\phi, \omega)$ is obtained, the role of trap motion can be studied explicitly and cooperation strategies determined.

Order ε^0. At the leading order of the expansion, the problem $u_0(x,t)$ satisfies

$$u_{0t} + u_{0xx} + 1 = 0, \quad -1 < x < 1; \quad u_{0x}(0) = u_{0x}(1) = 0, \quad u(x_j) = 0, \quad j = 1, 2\,, \tag{2.5}$$

which corresponds to the stationary solution in the absence of trap motion. The solution is t independent and given by

$$u_0(x) = \frac{1}{2}\begin{cases} -x^2 + x_1^2, & x \in \mathcal{R}_1(t); \\ -x^2 + (x_1 + x_2)x - x_0 x_1, & x \in \mathcal{R}_2(t); \\ (x_2 - x)(x_2 + x - 2), & x \in \mathcal{R}_3(t). \end{cases} \tag{2.6}$$

Order ε^1. In region $\mathcal{R}_1$, the boundary conditions on the correction term $u_1(x,t)$ are $u_{1x}(0) = 0$ together with

$$u_1(x_1) = -u_0'(x_1) f_1 = \frac{x_1}{2i}\left(e^{\omega_+^2 t} - e^{\omega_-^2 t}\right), \tag{2.7}$$

which gives rise to a correction equation featuring homogeneous solutions of

$$\phi_{xx} + \phi_t = 0, \qquad \phi(x,0) = \phi\Big(x, \frac{2\pi}{\omega}\Big). \tag{2.8a}$$

The general solution of (2.8a) which matches the boundary conditions (2.7) is

$$\begin{aligned} \phi(x,t;\omega) = {} & e^{\omega_-^2 t}\left[A_1 \cosh \omega_+ x + B_1 \sinh \omega_+ x\right] \\ & + e^{\omega_+^2 t}\left[A_2 \cosh \omega_- x + B_2 \sinh \omega_- x\right], \qquad \omega_\pm = \sqrt{\pm i\omega}, \end{aligned} \tag{2.8b}$$

for constants A_1, A_2, B_1, B_2. It is convenient to work with a complex form of the solution until the final result, at which point the real form is obtained. Fitting the relevant boundary conditions for $u_1(x_j)$ at $j = 1, 2$ gives the solutions in each region to be

$$u_1 = \frac{x_1}{2i}\left(e^{\omega_+^2 t}\frac{\cosh \omega_- x}{\cosh \omega_- x_1} - e^{\omega_-^2 t}\frac{\cosh \omega_+ x}{\cosh \omega_+ x_1}\right), \ x \in \mathcal{R}_1; \tag{2.9a}$$

$$\begin{aligned} u_1 = \frac{\ell}{4i}\Bigg(\frac{e^{\omega_+^2 t}}{\sinh \omega_- \ell}\left[\begin{array}{c} \sinh \omega_-(x - x_2) + \\ e^{\omega_-^2 \phi}\sinh \omega_-(x - x_1) \end{array}\right] \\ - \frac{e^{\omega_-^2 t}}{\sinh \omega_+ \ell}\left[\begin{array}{c} \sinh \omega_+(x - x_2) + \\ e^{\omega_+^2 \phi}\sinh \omega_+(x - x_1) \end{array}\right]\Bigg), \ x \in \mathcal{R}_2; \end{aligned} \tag{2.9b}$$

$$u_1 = \frac{x_2 - 1}{2i}\left(e^{\omega_+^2 t}\frac{\cosh \omega_-(x-1)}{\cosh \omega_-(x_2 - 1)}e^{\omega_-^2 \phi} - e^{\omega_-^2 t}\frac{\cosh \omega_+(x-1)}{\cosh \omega_+(x_2 - 1)}e^{\omega_+^2 \phi}\right), \ x \in \mathcal{R}_3, \tag{2.9c}$$

where $\ell = x_2 - x_1$. As $u_1(x,t)$ has zero mean over $t \in (0, \frac{2\pi}{\omega})$, it does not make a direct contribution to τ in (2.3). However, $u_{1x}(x_j)$ for $j = 1, 2$ contributes to τ through the boundary conditions on $u_2(x_j)$ given in (2.4b).

Order ε^2. Taking the general form $u_{1x}(x_j) = a_j e^{\omega_-^2 t} + b_j e^{\omega_+^2 t}$, where a_j and b_j are coefficients taken from (2.9), the boundary conditions on $u_2(x_j)$ from (2.4b) are

$$u_2(x_j) = -\frac{u_0''(x_j)}{2} f_1^2 - u_1'(x_j) f_1 = \frac{1}{2} - \frac{a_j}{2i} + \frac{b_j}{2i} + \mathcal{O}(e^{2\omega_\pm^2 t}) .$$

The general solution is therefore of form $u_2(x,t) = u_{2h}(x) + u_{2p}(x,t)$, where $u_{2p}(x,t)$ is the periodic component with zero mean over $t \in (0, \frac{2\pi}{\omega})$ and makes no contribution to the value of τ. Therefore only $u_{2h}(x)$ is required in each of the subregions. As u_{2h} satisfies a homogeneous Neumann condition in regions $\mathcal{R}_1, \mathcal{R}_3$, its value is constant in those regions, while in $\mathcal{R}_2$, Dirichlet conditions are applied at either end of the region resulting in a linear u_{2h}:

$$u_{2h} = \frac{1}{2} - \frac{x_1}{4} \left(\omega_+ \tanh \omega_+ x_1 + \omega_- \tanh \omega_- x_1 \right), \qquad x \in \mathcal{R}_1, \tag{2.10a}$$

$$\begin{aligned} u_{2h} = {} & \frac{(x - x_1)}{4} \left[\frac{\omega_+}{\sinh \omega_+ \ell} - \frac{\omega_-}{\sinh \omega_- \ell} \right] \sin \omega\phi \\ & + \frac{1}{4} - \frac{\ell}{8} \left[\frac{\omega_+}{\sinh \omega_+ \ell} \begin{pmatrix} \cosh \omega_+ \ell \\ + e^{i\omega\phi} \end{pmatrix} + \frac{\omega_-}{\sinh \omega_- \ell} \begin{pmatrix} \cosh \omega_- \ell \\ + e^{-i\omega\phi} \end{pmatrix} \right], \quad x \in \mathcal{R}_2, \end{aligned} \tag{2.10b}$$

$$u_{2h} = \frac{1}{2} - \frac{1 - x_2}{4} \left(\omega_+ \tanh \omega_+ (1 - x_2) + \omega_- \tanh \omega_- (1 - x_2) \right), \qquad x \in \mathcal{R}_3. \tag{2.10c}$$

The value of τ is calculated by integration in each subregion with application of Leibniz's rule. This gives

$$\tau = \frac{\omega}{2\pi} \int_0^{\frac{2\pi}{\omega}} \left[\int_{\mathcal{R}_1} u \, dx + \int_{\mathcal{R}_2} u \, dx + \int_{\mathcal{R}_3} u \, dx \right] dt = \tau_0 + \varepsilon^2 \tau_2 + \dots , \tag{2.11}$$

where, after much algebra and simplification of complex valued expressions, the final result

$$\tau_0 = \frac{x_1^2}{3} + \frac{(1 - x_2)^3}{3} + \frac{\ell^3}{12}; \tag{2.12a}$$

$$\begin{aligned} \tau_2 = {} & -\frac{\sqrt{2\omega} x_1^2}{4} \left(\frac{\sin \sqrt{2\omega} x_1 + \sinh \sqrt{2\omega} x_1}{\cos \sqrt{2\omega} x_1 + \sinh \sqrt{2\omega} x_1} \right) \\ & - \frac{\sqrt{2\omega}(1 - x_2)^2}{4} \left(\frac{\sin \sqrt{2\omega}(1 - x_2) + \sinh \sqrt{2\omega}(1 - x_2)}{\cos \sqrt{2\omega}(1 - x_2) + \sinh \sqrt{2\omega}(1 - x_2)} \right) \\ & + \frac{\ell}{2} + \frac{\sqrt{2\omega}\ell^2}{8} \left[\frac{\sin \sqrt{2\omega}\ell + \sinh \sqrt{2\omega}\ell}{\cos \sqrt{2\omega}\ell - \cosh \sqrt{2\omega}\ell} \right. \\ & \left. + 2 \left[\frac{\cosh \sqrt{\frac{\omega}{2}}\ell \sin \sqrt{\frac{\omega}{2}}\ell + \sinh \sqrt{\frac{\omega}{2}}\ell \cos \sqrt{\frac{\omega}{2}}\ell}{\cos \sqrt{2\omega}\ell - \cosh \sqrt{2\omega}\ell} \right] \cos \omega\phi \right], \end{aligned} \tag{2.12b}$$

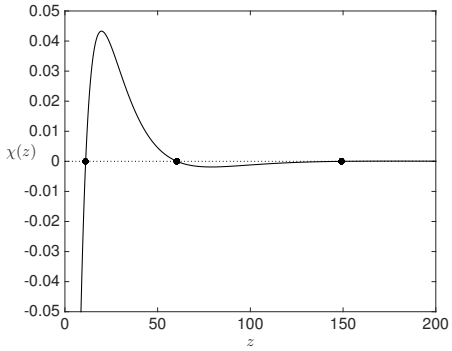

FIG. 4. *Plot of $\chi(z)$ from (2.13) with first three roots indicated. The MFPT is minimized by traps moving in phase when $\chi(\omega\ell^2) < 0$ and out of phase when $\chi(\omega\ell^2) < 0$.*

is obtained. Before proceeding to study the local extrema of τ, we first remark that τ_0 and τ_2 each contain three distinct contributions from each of the three intervals. In τ_0 and τ_2, the first two terms are contributions from the intervals $\mathcal{R}_1(t)$ and $\mathcal{R}_3(t)$, respectively, while the final terms are contributions associated with $\mathcal{R}_2(t)$. The local extrema of $\tau = \tau(\phi)$ are $\omega\phi = 0, \pi$ and correspond to the two traps being exactly in or out of phase with each other. The nature of these critical points is determined by

$$\frac{d^2\tau}{d\phi^2} = -\varepsilon^2 \frac{\sqrt{2}\omega^{\frac{5}{2}}\ell^2}{4}\chi(\omega\ell^2)\cos\omega\phi, \qquad \chi(z) = \left[\frac{\cosh\sqrt{\frac{z}{2}}\sin\sqrt{\frac{z}{2}} + \sinh\sqrt{\frac{z}{2}}\cos\sqrt{\frac{z}{2}}}{\cos\sqrt{2z} - \cosh\sqrt{2z}}\right]. \tag{2.13}$$

Therefore, the MFPT is minimized by the traps moving in phase ($\phi = 0$) when $\chi(\omega\ell^2) < 0$ and out of phase ($\phi = \pi/\omega$) when $\chi(\omega\ell^2) > 0$. The graph of $\chi(z)$ in Figure 4 indicates that its sign changes over certain intervals of $z = \omega\ell^2$. Applying a large argument approximation to $\chi(z_k) = 0$ implies that these thresholds behave asymptotically like

$$z_k \sim \frac{\pi^2}{8}(-1 + 4k)^2, \quad k = 1, 2, 3, \dots, \tag{2.14}$$

which agrees closely with values obtained from numerical solution of $\chi(z_k) = 0$ given in Table 1. Therefore, the optimal alignment strategy of the traps alternates as the quantity $\omega\ell^2$ increases. In the fast trap motion limit $\omega \to \infty$, the trap cooperation strategy is of diminished importantance since $\chi(\omega\ell^2) \to 0$ as $\omega \to \infty$. In the next section, we extend the analysis to an array of absorbing mobile traps in a bounded one-dimensional interval.

2.1. N traps in one dimension. The analysis of the previous section can easily be extended to accommodate N traps undergoing motion with relative phases

TABLE 1

Approximate (2.14) and numerical values for the critical $z = \omega\ell^2$ over which the optimal cooperation strategy changes.

	z_1	z_2	z_3
Approximate	11.1033	60.4513	149.2778
Numerical	11.1866	60.4517	149.2778

to one another. The one-dimensional domain (x_1, x_N) is expressed as union of $N-1$ intervals $\cup_{j=1}^{N-1}\mathcal{R}_j(t)$, where

$$\mathcal{R}_j(t) = (x_j + \varepsilon f_j(t), x_{j+1} + \varepsilon f_{j+1}(t)), \qquad f_j(t) = \sin\omega(t-\phi_j), \qquad \ell_j = x_{j+1} - x_j.$$

In this case we stipulate that all traps, including the end points, are absorbing so that

$$u(x_j + \varepsilon f_j(t), t) = 0, \qquad j = 1, \dots N. \tag{2.15}$$

We assume the cooperation phases ϕ_j are free variables over which to optimize. The process for obtaining the regular expansion solution of (2.1) with trapping conditions (2.15) as $\varepsilon \to 0$ is identical to that of section 2. In particular, the solution over each interval $\mathcal{R}_j$ can be solved in terms of the phase difference between the boundary points x_j, x_{j+1}. As such, the contributions to the MFPT τ from each individual cell are exactly analogous to the contribution of the central region $\mathcal{R}_2$ in (2.12). Therefore, the same process yields that as $\varepsilon \to 0$,

$$\tau = \sum_{j=1}^{N-1} \frac{\ell_j^3}{12} + \varepsilon^2 \sum_{j=1}^{N-1} \left[\frac{\ell_j}{2} + \frac{\sqrt{2\omega}\ell_j^2}{8} \left(\frac{\sin\sqrt{2\omega}\ell_j + \sinh\sqrt{2\omega}\ell_j}{\cos\sqrt{2\omega}\ell_j - \cosh\sqrt{2\omega}\ell_j} + 2\chi(\omega\ell_j^2)\cos\omega(\phi_{j+1} - \phi_j) \right) \right] + \mathcal{O}(\varepsilon^2), \tag{2.16}$$

where $\ell_j = x_{j+1} - x_j$. In Figure 5 we display a numerical comparison of this formula for $N = 2$ with the MFPT obtained from full numerical simulation of (2.2) and observe close agreement. Additionally, we numerically observe the optimal cooperation strategy switching over when $\omega\ell^2 = z_1 \approx 11.1866$ as determined from the roots of $\chi(z)$ in (2.13).

When the intervals have common length, $\ell_j = \ell$ for $j = 1, \dots, N-1$, the conclusions are the same as the two-trap case, i.e., the MFPT is minimized by moving in phase with the neighboring trap if $\chi(\omega\ell^2) < 0$ and out of phase with neighboring traps if $\chi(\omega\ell^2) > 0$. For nonuniform spacing, finding the lowest MFPT is reduces to minimizing $f(s_1, \dots, s_n) = \sum_{j=1}^n a_j \cos s_j$ for $s_j \in (0, 2\pi)$. The global minimum of this function is $-\sum_{j=1}^n |a_j|$, which is attained when $s_j = 0$ if $a_j < 0$ and $s_j = \pi$ if $a_j > 0$. Consequently, the cooperation strategy of N traps which minimizes the MFPT (2.16) up to $\mathcal{O}(\varepsilon^2)$ is

$$\phi_{j+1} - \phi_j = \begin{cases} 0 & \text{if} \quad \chi(\omega\ell_j^2) < 0; \\ \dfrac{\pi}{\omega} & \text{if} \quad \chi(\omega\ell_j^2) > 0, \end{cases} \tag{2.17}$$

with a corresponding minimum MFPT $\tau_{\min}$

$$\tau_{\min} = \sum_{j=1}^{N-1} \frac{\ell_j^3}{12} + \varepsilon^2 \sum_{j=1}^{N-1} \left[\frac{\ell_j}{2} + \frac{\sqrt{2\omega}\ell_j^2}{8} \left(\frac{\sin\sqrt{2\omega}\ell_j + \sinh\sqrt{2\omega}\ell_j}{\cos\sqrt{2\omega}\ell_j - \cosh\sqrt{2\omega}\ell_j} - 2|\chi(\omega\ell_j^2)| \right) \right] + \mathcal{O}(\varepsilon^2), \tag{2.18}$$

as $\varepsilon \to 0$. Similarly, the global MFPT τ is maximized by adopting the opposite phase cooperation strategy to (2.17).

2.2. Adaptation to neighboring traps. As a demonstration of this theory in which the optimal strategy is not exactly in phase or out of phase, we suppose a fixed configuration of traps is present with common frequency ω and individual phases.

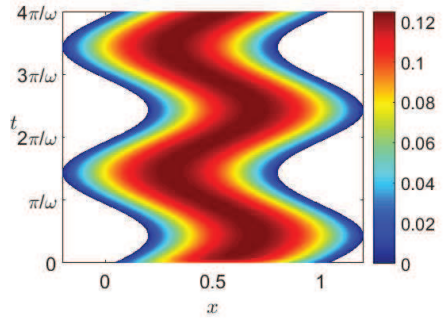

(a) Numerical solution of (2.2) over two periods with two in phase mobile absorbing boundary traps. Parameters $\ell = 1$, $\omega = 1$, $\varepsilon = 0.2$ and $\phi = 0$.

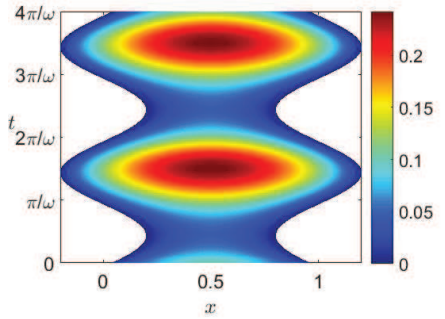

(b) Numerical solution of (2.2) over two periods with two out of phase mobile absorbing boundary traps. Parameters $\ell = 1$, $\omega = 1$, $\varepsilon = 0.2$ and $\phi = \pi/\omega$.

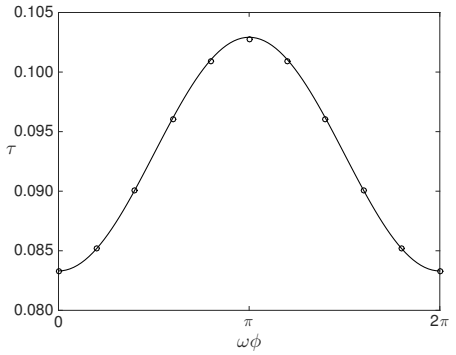

(c) τ against $\omega\phi$ for $N = 2$, $\omega = 1$, $\varepsilon = 0.2$ and $\ell = 1$, ($\omega\ell^2 = 1$). Asymptotic (solid) and numerical solutions (circles).

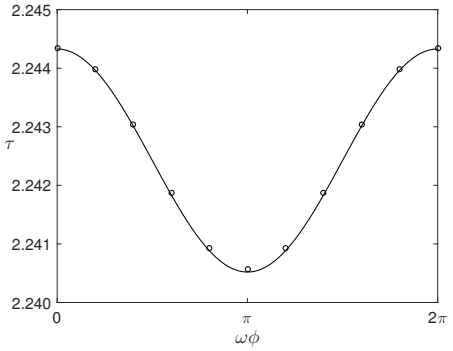

(d) τ against $\omega\phi$ for $N = 2$, $\omega = 2$, $\varepsilon = 0.1$, and $\ell = 3$ ($\omega\ell^2 = 18$). Asymptotic (solid) and numerical solutions (circles).

FIG. 5. (a), (b) *Numerical solutions of* (2.1) *for two in-phase (top left) and out-of-phase (top right) traps.* (c), (d) *Agreement of numerical simulations and asymptotic theory as the phase difference between the two traps varies. When* $\omega\ell^2 = 1$*, the MFPT is minimized at* $\phi = 0$ *(bottom left) and for* $\omega\ell^2 = 18$*, an out-of phase strategy* $\omega\phi = \pi$ *minimizes the MFPT (bottom right).*

We then insert an additional trap of frequency ω at location x_k with phase ϕ_k. The contribution to the MFPT τ which depends only on the phase ϕ_k of the additional trap is

(2.19)
$$\mathcal{I}_k = \frac{\varepsilon^2}{\sqrt{8\omega}} \left[z_k \cos\omega(\phi_{k+1} - \phi_k) + z_{k-1} \cos\omega(\phi_k - \phi_{k-1}) \right], \qquad z_k = \omega\ell_k^2\, \chi(\omega\ell_k^2),$$

where x_{k+1} and x_{k-1} are the locations of the traps adjacent to the inserted one. Assuming ϕ_{k-1} and ϕ_{k+1} are fixed, the local extrema of this interaction function are the two solutions $\phi_k^{\pm} \in (0, 2\pi/\omega)$ of the equation

(2.20)
$$\tan\omega\phi_k^{\pm} = \frac{z_k \sin\omega\phi_{k+1} + z_{k-1} \sin\omega\phi_{k-1}}{z_k \cos\omega\phi_{k+1} + z_{k-1} \cos\omega\phi_{k-1}}.$$

Therefore, the optimal interaction strategies are not simply in or out of phase with the adjacent traps but are determined by a weighted average of their phases. The

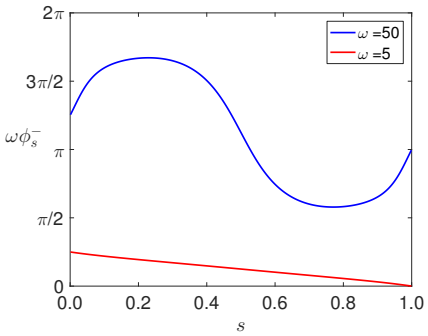

(a) The phase $\omega\phi_s$ minimizing the MFPT for a trap inserted at location s for $\omega = 5, 50$.

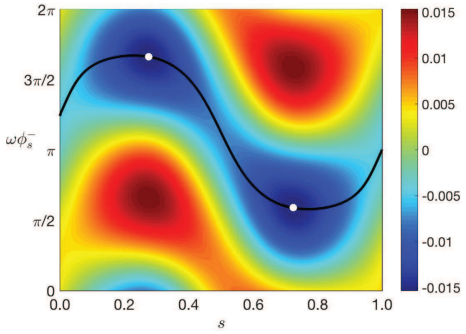

(b) The full landscape $\mathcal{I}(s, \omega\phi)$ for $\omega = 50$.

FIG. 6. *Optimization of the MFPT by adapting to the phase of neighboring traps. Left panel: For a trap inserted at fixed location $s \in (0,1)$ between two traps located at $x = 0, 1$ and phases $\phi = 0, \pi/4\omega$, the minimizing phase $\omega\phi_s^-$ is plotted as a function of s for $\omega = 5$ and $\omega = 50$. Curves obtained from solution of (2.21). Right panel: For the case $\omega = 50$, the full landscape $\mathcal{I} = \mathcal{I}(s, \omega\phi)$, defined in (2.19), is shown for $\varepsilon = 0.2$ with the minimizing phase overlaid (black curve). The two global minima are indicated with open white circles at $(s, \omega\phi) \approx (0.2750, 5.2255)$ and $(s, \omega\phi) \approx (0.7250, 1.8551)$.*

nature of each local extrema follows from the sign of

$$\frac{d^2\mathcal{I}_k}{d^2\phi_k}(\phi_k^{\pm}) = -\omega^2\mathcal{I}_k(\phi_k^{\pm}) = -\frac{\varepsilon^2\omega^{\frac{3}{2}}}{\sqrt{8}} \sec\omega\phi_k^{\pm} \left[z_k \cos\omega\phi_{k+1} + z_{k-1}\cos\omega\phi_{k-1}\right].$$

As an example, consider two mobile traps centered at $x = 0, 1$ with fixed phases $\omega\phi = 0, \frac{\pi}{4}$, respectively, and common frequency ω. An additional mobile trap is centered at location $0 < s < 1$ with phase ϕ_s and frequency ω. From (2.20), the optimizing values of ϕ_s satisfy

$$\tan\omega\phi_s^{\pm} = \frac{(1-s)^2\chi(\omega(1-s)^2)\sin\frac{\pi}{4}}{(1-s)^2\chi(\omega(1-s)^2)\cos\frac{\pi}{4} + s^2\chi(\omega s^2)}. \tag{2.21}$$

In Figure 6, we display the solution of (2.21) for values of $\omega = 5$ and $\omega = 50$. The optimal adaptation strategy is observed to depend quite sensitively on the frequency ω and the spatial placement of the trap.

3. *N* traps on a unit disk. In this section, we seek optimal cooperation strategies for two small identical mobile traps in a bounded two-dimensional domain. In particular, we consider the scenario in which the two mobile traps perform a search for a particle diffusing inside the reflective unit disk Ω by rotating around the center of the disk at a constant angular frequency ω. We first derive the two-dimensional analogue of the one-dimensional MFPT problem (2.2) with a single mobile absorbing trap undergoing $2\pi/\omega$-periodic motion. We let Ω be any arbitrary bounded two-dimensional domain over which the search is conducted. The set of points occupied by the trap are denoted $\Omega_{\text{trap}}(z) \subset \Omega$, which indicates the shape and location of the trap at time z while satisfying the periodicity condition $\Omega_{\text{trap}}(z) = \Omega_{\text{trap}}(z + 2\pi/\omega)$. The particle location $\mathbf{x} = (x, y)$ at time z thus takes on the values $\mathbf{x} \in \Omega \setminus \Omega_{\text{trap}}(z)$. The particle

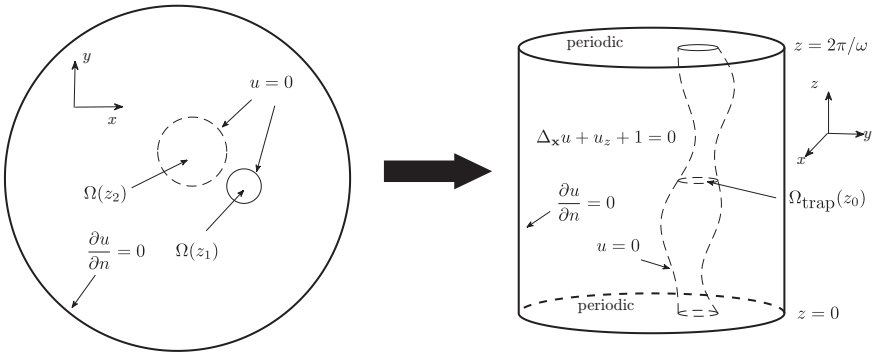

FIG. 7. *Schematic of transforming the moving two-dimensional problem to a static three-dimensional problem. In the two-dimensional schematic on the left, $\Omega(z_1)$ and $\Omega(z_2)$ show the location and size of the trap at times $z = z_1$ and $z = z_2$, respectively. In the three-dimensional schematic on the right, the motion of the random particle is diffusive in the x–y plane with a deterministic drift in the positive z direction. The quantity $u(\mathbf{x}, z)$ gives the mean time to capture of a random particle starting at location $\mathbf{x}$ by a mobile trap beginning its periodic motion with configuration $\Omega_{trap}(z)$.*

is absorbed at time z when $\mathbf{x} \in \partial\Omega_{\text{trap}}(z)$. See the left panel in Figure 7. In this way, the particle undergoes a random walk in the $\mathbf{x}$ directions with a deterministic drift in the z direction. For a particle located at $\mathbf{x}$ at time z, its MFPT $u(\mathbf{x}, z)$ is then an average of the MFPT associated with all the locations it can possibly occupy at time $z + \Delta z$ plus the Δz time it takes to get there. That is,

(3.1)
$$u(x,y,z) = \frac{1}{4}\left[u(x+\Delta x, y, z+\Delta z) + u(x-\Delta x, y, z+\Delta z) + u(x, y+\Delta y, z+\Delta z) + u(x, y-\Delta y, z+\Delta z)\right] + \Delta z\,; \qquad u = 0\,, \quad \mathbf{x} \in \Omega_{\text{trap}}(z).$$

Expanding for small Δx, Δy, and Δz, and taking the usual limit $\Delta x = \Delta y \to 0$ and $\Delta z \to 0$ with $\Delta z \sim \Delta x^2 = \Delta y^2$, we obtain the three-dimensional boundary value problem for the MFPT $u(\mathbf{x}, z)$

$$\Delta_{\mathbf{x}} u + u_z + 1 = 0\,, \qquad \mathbf{x} = (x,y) \in \Omega \setminus \Omega_{\text{trap}}(z)\,, \quad z \in [0, 2\pi/\omega)\,, \tag{3.2a}$$

$$u = 0\,, \quad \mathbf{x} \in \partial\Omega_{\text{trap}}(z)\,, \qquad \partial_n u = 0\,, \quad \mathbf{x} \in \partial\Omega\,, \quad z \in [0, 2\pi/\omega)\,, \tag{3.2b}$$

$$u(\mathbf{x}, 0) = u(\mathbf{x}, 2\pi/\omega)\,, \quad \mathbf{x} \in \Omega \setminus \Omega_{\text{trap}}(0)\,. \tag{3.2c}$$

In (3.2), $\Delta_{\mathbf{x}} \equiv \partial^2/\partial x^2 + \partial^2/\partial y^2$, and we have assumed periodicity of the trap's motion $\Omega_{\text{trap}}(z + 2\pi/\omega) = \Omega_{\text{trap}}(z)$. The motion of the random particle is therefore diffusive in the x–y plane with a deterministic drift in the positive z direction. The quantity $u(\mathbf{x}, z)$ gives the mean time to capture of a random particle starting from location $\mathbf{x}$ by a mobile trap beginning its periodic motion with configuration $\Omega_{\text{trap}}(z)$. The schematic of this three-dimensional problem is shown in the right panel of Figure 7. We remark that the derivation generalizes easily to N mobile traps each undergoing $2\pi/\omega$-periodic motion. Analysis of (3.2) is in general very difficult. We therefore consider the special case in which the N traps rotate at the same frequency about the center of a unit disk. With this rotational symmetry, the geometry of the corresponding PDE remains two-dimensional. A detailed derivation of the PDE for a single

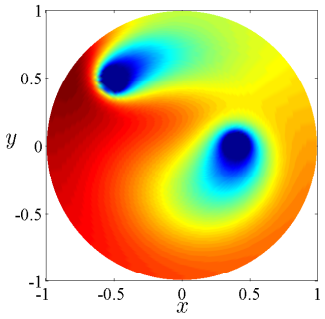

FIG. 8. *A typical two-trap solution with $\varepsilon = 0.1$, $\omega = 30$, $r_1 = 0.3$, $r_2 = 0.7$, and $\theta_2 = 3\pi/4$. Blue (red) regions indicate small (large) values of u. Notice that the MFPT is lower in front of the rotating traps than it is behind. Computed using the finite element software FlexPDE.*

rotating trap is given in [32], which we generalize here for N rotating traps. In the frame of N traps each rotating clockwise about the center of the disk with common frequency ω, we obtain the mixed Neumann–Dirichlet boundary value problem

$$\Delta u + \omega u_\theta + 1 = 0\,, \qquad \mathbf{x} \in \Omega \setminus \cup_{j=1}^{N} \Omega_{\varepsilon_j}\,; \tag{3.3a}$$

$$u = 0\,, \quad \mathbf{x} \in \partial\Omega_a = \cup_{j=1}^{N} \partial\Omega_{\varepsilon_j}\,, \quad j = 1, \dots, N\,; \qquad \partial_n u = 0\,, \quad \mathbf{x} \in \partial\Omega\,, \tag{3.3b}$$

where u_θ is the derivative of u with respect to the angular coordinate θ. In (3.3), Δ denotes the Laplacian with respect to the polar coordinates (r, θ), $\partial\Omega_a$ the union of the absorbing boundaries of N small traps separated by $\mathcal{O}(1)$ distance, $\partial\Omega$ the reflective outer boundary of the disk, and $u(\mathbf{x})$ the nondimensional MFPT of a random walker starting from location $\mathbf{x}$ to one of the traps. The jth trap $\Omega_{\varepsilon_j} = \mathbf{x}_j + \varepsilon\Omega_{0j}$ is centered at location $\mathbf{x}_j$, where Ω_{0j} is the $\mathcal{O}(1)$ geometry of the trap and ε is its "radius." The schematic and a typical solution (computed using the finite element software FlexPDE [1]) are shown in Figures 1(b) and 8, respectively.

Assuming a uniform distribution of starting locations, the average MFPT (sometimes referred to as global MFPT) is the quantity

$$\bar{u} = \frac{1}{|\Omega|} \int_\Omega u(\mathbf{x})\, d\Omega\,, \tag{3.4}$$

where $|\Omega|$ is the size of the domain. Below, we calculate $\bar{u}$ in terms of the trap locations $\mathbf{x}_j$. We then optimize $\bar{u}$ with respect to the locations. To reduce the number of parameters in the optimization problem, we assume that all traps are circular and share a common radius ε, i.e., Ω_{0j} are disks of unit radius for each $j = 1, \dots, N$.

3.1. The regime $\boldsymbol{\omega \sim \mathcal{O}(1)}$. In the regime $\omega \sim \mathcal{O}(1)$, we adopt the method of matched asymptotic expansions [23, 21] to calculate $\bar{u}$ as a function of the relative locations $\mathbf{x}_j$ of N traps. In the inner region near the jth trap, we let $\mathbf{y} = |\mathbf{x} - \mathbf{x}_j|/\varepsilon$ and $u(\mathbf{x}_j + \varepsilon y) = U_j(\mathbf{y})$ to obtain the leading order inner problem

$$\Delta U_j = 0\,, \qquad \mathbf{y} \in \mathbb{R}^2 \setminus \Omega_{0j}\,, \qquad U_j \sim S_j \log|\mathbf{y}| - S_j \log d_j \ \text{ as } \ |\mathbf{y}| \to \infty\,. \tag{3.5}$$

In (3.5), d_j is referred to as the logarithmic capacitance of the jth trap, which depends on the geometry Ω_{0j}. A list of numerical and analytic values of d_j for different shapes is given in [24]. For the case we consider, where Ω_{0j} is the unit disk, $d_j = 1$ so that

$U_j = S_j \log|\mathbf{y}|$ is the exact solution of (3.5). The quantity S_j, the strength of trap j, is to be determined from a system of linear equations obtained by matching inner and outer solutions. In terms of the outer variables, we calculate the matching condition

$$u \sim S_j \log|\mathbf{x}-\mathbf{x}_j| - S_j \log\varepsilon \ \text{ as } \ \mathbf{x}\to\mathbf{x}_j\,. \tag{3.6}$$

Since u is logarithmic near each trap, we may express u as a sum of Neumann Green's functions $G(\mathbf{x},\mathbf{x}_0)$ satisfying

$$\Delta G + \omega G_\theta = \frac{1}{|\Omega|} - \delta(\mathbf{x}-\mathbf{x}_0)\,, \qquad \mathbf{x}\in\Omega; \tag{3.7a}$$

$$\partial_n G = 0, \qquad \mathbf{x}\in\partial\Omega\,, \qquad \int_\Omega G\,d\Omega = 0\,, \tag{3.7b}$$

$$G \sim -\frac{1}{2\pi}\log|\mathbf{x}-\mathbf{x}_0| + R(\mathbf{x}_0,\mathbf{x}_0) \ \text{ as } \ \mathbf{x}\to\mathbf{x}_0\,. \tag{3.7c}$$

Then in the limit $\varepsilon\to 0$, we write

$$u = -2\pi\sum_{j=1}^{N} S_j G(\mathbf{x},\mathbf{x}_j) + \bar{u}\,. \tag{3.8}$$

In (3.7c), $R(\mathbf{x}_0,\mathbf{x}_0)$ is the regular part of G as $\mathbf{x}\to\mathbf{x}_0$, referred to as the self-interaction term. By the integral condition in (3.7b), which uniquely specifies G, $\bar{u}$ in (3.8) is the uniform average of u in (3.4) that we seek to optimize. To obtain the $N+1$ equations for $S_1,\dots,S_N$ and $\bar{u}$, we first compare (3.8) with (3.7) to (3.3) to obtain the solvability condition

$$\sum_{j=1}^{N} S_j = \frac{1}{2}\,. \tag{3.9}$$

The other N equations come from applying the matching condition (3.6) at the N trap locations $\mathbf{x}_j$. Letting $\mathbf{x}\to\mathbf{x}_i$ in (3.8) and using the limiting behavior of G near $\mathbf{x}_i$, we calculate

$$-2\pi S_i\left[-\frac{1}{2\pi}\log|\mathbf{x}-\mathbf{x}_i|+R_{ii}\right] - 2\pi\sum_{j\neq i}^{N} G_{ij}S_j + \bar{u} = S_i\log|\mathbf{x}-\mathbf{x}_i| + \frac{S_i}{\nu}\,, \quad i=1,\dots,N, \tag{3.10}$$

where $R_{ii}\equiv R(\mathbf{x}_i,\mathbf{x}_i)$, $G_{ij}\equiv G(\mathbf{x}_i,\mathbf{x}_j)$, and $\nu\equiv -1/\log\varepsilon \ll 1$. The logarithmic terms in (3.10) match by construction. To write (3.10) in matrix form, we define

$$\mathbf{s}\equiv\begin{pmatrix} S_1\\ \vdots\\ S_N\end{pmatrix},\ \mathbf{e}\equiv\begin{pmatrix}1\\ \vdots\\ 1\end{pmatrix},\ \mathcal{E}\equiv\mathbf{e}\mathbf{e}^t,\ \mathcal{G}\equiv\begin{pmatrix} R_{11} & G_{12} & \cdots & G_{1N}\\ G_{21} & \ddots & \ddots & \vdots\\ \vdots & \ddots & \ddots & G_{N-1,N}\\ G_{N1} & \cdots & G_{N,N-1} & R_{NN}\end{pmatrix}, \tag{3.11}$$

where t denotes the transpose and $\mathcal{G}$ in (3.11) is the Green's interaction matrix, which encodes information on the locations of the N traps. In contrast to the Green's matrix

in [21], $\mathcal{G}$ is not symmetric due to the symmetry-breaking rotation of the traps. We rewrite (3.9) and (3.10) in the form

$$2\pi\mathcal{G}\mathbf{s} + \frac{1}{\nu}\mathcal{I}\mathbf{s} = \bar{u}\mathbf{e}\,, \qquad \mathbf{e}^t\mathbf{s} = \frac{1}{2}\,, \tag{3.12}$$

where $\mathcal{I}$ is the $N \times N$ identity matrix. Multiplying both sides of (3.12) by $\mathbf{e}^t$ and solving for $\bar{u}$, we obtain the solution for $\bar{u}$ and the strengths of the traps $S_1, \ldots, S_N$

$$\bar{u} = \frac{1}{N}\left[2\pi\mathbf{e}^t\mathcal{G}\mathbf{s} + \frac{1}{2\nu}\right], \qquad \mathbf{s} = \frac{1}{2\nu N}\left[2\pi\left(\mathcal{I} - \frac{1}{N}\mathcal{E}\right)\mathcal{G} + \frac{1}{\nu}\mathcal{I}\right]^{-1}\mathbf{e}\,. \tag{3.13}$$

We observe in (3.13) that $S_j = (2N)^{-1}$ to leading order in ν^{-1} for all j, and $\bar{u} = (2\nu N)^{-1}$. That is, all traps share a common strength to leading order, and $\bar{u}$ increases logarithmically as $\varepsilon \to 0$. The effect of trap locations on $\bar{u}$ is therefore a smaller $\mathcal{O}(1)$ correction.

To construct the Green's interaction matrix (3.11) in the case $\omega \neq 0$, we adopt a Fourier series approach where we let $\mathbf{x} = (r\cos\theta, r\sin\theta)$. The Neumann Green's function satisfying (3.7) is then given by [32]

$$G(\mathbf{x}, \mathbf{x}_0; \omega) = G(r, \theta, r_0, \theta_0; \omega) = R_0(r, r_0) + \sum_{m>0} e^{im(\theta-\theta_0)} R_m(r, r_0) + \text{c.c.}\,, \tag{3.14a}$$

where the coefficients R_0 and R_m are given by

$$R_0(r, r_0) = \frac{r^2}{4\pi} + \frac{1}{8\pi}[2r_0^2 - 3] - \frac{1}{2\pi}\begin{cases} \log r_0\,, & 0 < r < r_0, \\ \log r\,, & r_0 < r < 1, \end{cases} \tag{3.14b}$$

$$R_m(r, r_0; \omega) = \frac{1}{2\pi}\begin{cases} \left[-\dfrac{K_m'(c_m)}{I_m'(c_m)} I_m(c_m r_0) + K_m(c_m r_0)\right] \\ \qquad \times I_m(c_m r), \quad 0 < r < r_0, \\ \left[-\dfrac{K_m'(c_m)}{I_m'(c_m)} I_m(c_m r) + K_m(c_m r)\right] \\ \qquad \times I_m(c_m r_0)\,, \quad r_0 < r < 1, \end{cases} \qquad c_m \equiv -i\sqrt{im\omega}\,, \tag{3.14c}$$

where $K_m(z)$ and $I_m(z)$ are modified Bessel functions of the first and second kind. The regular part of G is obtained by using the definition in (3.7c) and expressing $\log|\mathbf{x} - \mathbf{x}_0|$ in terms of its Fourier series. This calculation yields

$$R(\mathbf{x}_0; \mathbf{x}_0) = \frac{r_0^2}{2\pi} - \frac{3}{8\pi} + \sum_{m>0}\left(R_m(r_0, r_0) - \frac{1}{4\pi m}\right) + \text{c.c.} \tag{3.14d}$$

In (3.14), c.c. refers to the complex conjugate of the term involving the summation. In the case where ω, ε are fixed and $N = 2$, we compare in Figure 9 the asymptotic result (3.13) for $\bar{u}$ to full numerical solutions of (3.3) obtained using FlexPDE. In Figure 9(a), we let the polar coordinates of the first trap be $(r_1, \theta_1) = (0.4, 0)$, with the second located at various locations on the ring $r_2 = 0.8$. In Figure 9(b), we fix the angle of the second trap at $\theta_2 = \pi$ and vary r_2 between 0 and 1. In both figures, we observe excellent agreement between the asymptotic formula (3.13) and numerical results.

Using the MATLAB global optimization algorithm `GlobalSearch` with `fmincon()`, we optimize $\bar{u}$ in (3.13) over r_1, r_2, and θ_2, where, without loss of generality, we set the

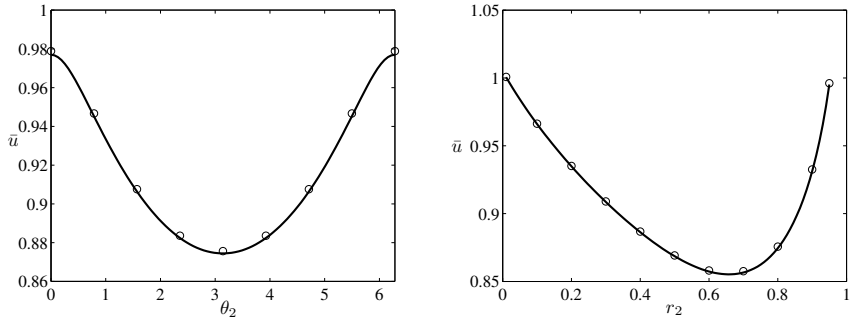

(a) $\bar{u}$ versus θ_2. (b) $\bar{u}$ versus r_2.

FIG. 9. *Comparison of the asymptotic formula for* $\bar{u}$ (3.13) *(solid curve) versus numerical results obtained from a finite elements solution of* (3.3) *(circles) with parameter values* $\omega = 5$ *and* $\varepsilon = 0.01$. *In both figures, the first trap is located at* $(r_1, \theta_1) = (0.4, 0)$, *while the location of the second* (r_2, θ_2) *is varied.* (a) $r_2 = 0.8$, *while* θ_2 *is varied.* (b) $\theta_2 = \pi$, *while* r_2 *is varied.*

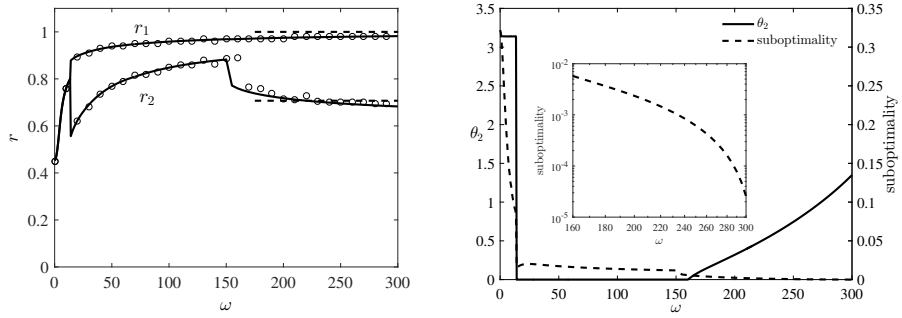

(a) Optimal radii of rotation. (b) Optimal relative phase.

FIG. 10. *Optimal radii of rotation* (a) *along with relative phase and minimum* $\bar{u}$ (b) *obtained from optimizing* (3.13) *for a range of* ω *using the* MATLAB *global optimization algorithm* `GlobalSearch` *with* `fmincon()` *(solid). Here,* $\varepsilon = 1 \times 10^{-4}$. *Open circles indicate optimal results obtained from an exhaustive search over the entire (discretized) parameter space* (r_1, r_2, θ_2). *For* $\omega \lesssim 14$, *the optimal configuration consists of two traps rotating* π*-phase apart at the same radius. For* $14 \lesssim \omega \lesssim 160$, *the optimal configuration has the traps rotating exactly in phase but on two different rings. The dashed lines in* (a) *represent the limiting behavior in the subregime* $\mathcal{O}(1) \ll \omega \ll \mathcal{O}(\varepsilon^{-1})$. *In* (b), *we observe that for* $\omega \gtrsim 160$, *the phase difference becomes nonzero while the traps remain on two different rings. With the dashed line on the right axis, we plot by how much the average MFPT increases (as a fraction of the optimal value) when* θ_2 *is chosen to be* π *(*$\pi - 0.1$ *when* $\omega \lesssim 14$*) radians from its optimizing value. The inset plots the suboptimality on a log-log scale, showing that it decreases rapidly as* ω *becomes large. The favorably similar results of the exhaustive search have been excluded in* (b) *to avoid clutter.*

angular location of one of the traps at $\theta_1 = 0$. The results are shown in solid curves in Figure 10. With open circles in Figure 10(a), we indicate optimal results obtained from an exhaustive search over the entire (discretized) paramter space (r_1, r_2, θ_2). The corresponding results for θ_2 have been omitted in Figure 10(b) to avoid clutter. For $\omega \lesssim 14$, the optimal configuration consists of two traps rotating π-phase apart at equal radius. For $14 \lesssim \omega \lesssim 160$, the optimal configuration has the traps rotating exactly in phase ($\theta_2 = 0$) but on two well-separated different rings. This "bifurcation"

is analogous to that found in [32] for one rotating trap, where the optimal radius of rotation is nonzero only when $\omega \gtrsim 3$. The key difference, however, is that since a zero radius of rotation implies that the trap remains stationary, rotation in the one trap case can be *detrimental* to search times when ω is small. That is, one observes a decrease in the optimal MFPT only when $\omega \gtrsim 3$. In contrast, we observe for this two-trap configuration that the optimal MFPT is a decreasing function of ω for any ω (not shown). For $\omega \gtrsim 160$, the optimal phase difference again becomes nonzero, but the two traps remain on different rings.

With the dashed line in Figure 10(b), we plot by how much the average MFPT increases (as a fraction of its optimal value) when the relative phase is chosen to be π ($\pi - 0.1$ when $\omega \lesssim 14$) radians from its optimal value. The inset plots the suboptimality on a log-log scale, showing that it decreases rapidly as ω becomes large, as expected. We remark that the leading order value of $\bar{u}$ as given by (3.4) is $\bar{u} \sim (2\pi\nu N)^{-1}$, while its dependence on r_1, r_2, and the phase θ_2 appears at $\mathcal{O}(1)$. As such, the fraction by which a suboptimal MFPT exceeds the optimal value is of order $\mathcal{O}(\nu)$. However, since $\nu = -1/\log\varepsilon$ can be rather large even when ε is small, the improvement of choosing an optimal over suboptimal configuration can be nontrivial. For example, with $\varepsilon = 1 \times 10^{-4}$ in Figure 10(b), choosing a suboptimal phase increased the MFPT by $\sim 11\%$ when $\omega = 10$.

We note that in the small $\omega \to 0$ limit of Figure 10(a), the result is the same as that obtained from optimizing $\bar{u}$ with the Neumann Green's function and its regular part (3.14) replaced by their $\omega = 0$ variants [21]. For large ω, the optimal radii approach $r_1 = 1/\sqrt{2}$ and $r_2 = 1$, represented by the dashed lines. In this limit, the accuracy of the truncated sum of (3.14d) is diminished due to numerical under- and overflow. In section 3.2, we adopt a different approach for calculating $\bar{u}$ in this particular large ω regime that does not involve a infinite sum. We use it to demonstrate the result suggested by the dashed lines in Figure 10(a) and extend it to N traps.

3.2. The subregime $\mathcal{O}(1) \ll \omega \ll \mathcal{O}(\varepsilon^{-1})$. In section 3.1, optimal configurations could only be found through numerical optimization of a function involving a truncated series. It is thus very difficult to understand how the optimal radii of rotation behave in the limit of large ω. Here, we use a leading order expression for the Neumann Green's function to calculate a closed form expression for the objective function $\bar{u}$. This simplified result allows the limiting behavior of the optimal radii shown in Figure 10(a) to be calculated explicitly. We note that this is not a distinguished regime, as it is contained within the $\omega \sim \mathcal{O}(1)$ regime. In that sense, we consider ω as being fixed at a very large value while ε is sent to 0. In this limit, a trap rotating on the ring of radius r_0 can be thought of as being almost everywhere on that ring at once. This near-radial symmetry was exploited in [32], where a matched asymptotics approach was employed to compute the leading order radially symmetric solution of (3.7)

$$G(r, r_0) = \frac{r^2 - r_0^2}{4\pi} - \frac{1}{2\pi}\Theta(r - r_0)\log\left(\frac{r}{r_0}\right) + \hat{H}\,, \tag{3.15a}$$

where $\Theta(z)$ is the Heaviside step function and

$$\hat{H}(r_0) \sim -\frac{1}{\pi}\left[-\frac{r_0^2}{2} + \frac{3}{8} + \frac{1}{2}\log r_0\right]. \tag{3.15b}$$

From a separately constructed inner solution, the limiting behavior of G

$$G(r, r_0) \sim \frac{1}{2\pi}\left[-\log|\mathbf{x}-\mathbf{x}_0| - \log\left(\frac{r_0\omega}{4}\right) - \gamma\right] + \hat{H}\,, \quad \text{as} \quad \mathbf{x}\to\mathbf{x}_0\,, \tag{3.16}$$

yields the leading order regular part of G

$$R(r_0) \sim \frac{1}{2\pi}\left[-\log\left(\frac{r_0\omega}{4}\right) - \gamma\right] + \hat{H}(r_0)\,. \tag{3.17}$$

In (3.16), γ is Euler's constant. Recalling that $\mathbf{s} = (2N)^{-1}\mathbf{e}$ to leading order in ν, we calculate the simplified leading order formula for $\bar{u}$

$$\bar{u} = \frac{1}{2\nu N} + \frac{\pi}{N^2}\sum_{ij}\mathcal{G}_{ij} + \mathcal{O}(\nu)\,, \tag{3.18}$$

where $\mathcal{G}_{ij}$ is the ijth entry of the matrix $\mathcal{G}$ defined in (3.11). For $N = 2$, assuming $r_1 < r_2$, we use (3.15) to calculate

$$\bar{u} = \frac{1}{4\nu} + \frac{1}{8}\left[\log\left(\frac{16}{\omega^2}\right) - 2\gamma - 3 + 2(r_1^2 + r_2^2) - 2\log r_1 - 4\log r_2\right] + \mathcal{O}(\nu)\,. \tag{3.19}$$

Finding the critical points of (3.19) by solving $\partial_{r_1}\bar{u} = \partial_{r_2}\bar{u} = 0$ leads to two uncoupled equations for r_1 and r_2. The result is that $\bar{u}$ is minimized to leading order when r_1 and r_2 are given by

$$r_1 \sim \frac{1}{\sqrt{2}}\,, \qquad r_2 \sim 1\,, \quad \text{as } \omega\to\infty \text{ with } \omega \ll \mathcal{O}(\varepsilon^{-1})\,. \tag{3.20}$$

We make three remarks. The first is that result (3.20) is rather counterintuitive given the suboptimal nature of search locations near boundaries. However, it was shown also in the same subregime $\mathcal{O}(1) \ll \omega \ll \mathcal{O}(\varepsilon^{-1})$ that a single rotating trap is best placed asymptotically close to the boundary of the unit disk [32]. Second, in assuming radial symmetry in constructing G in (3.16), we have lost resolution on θ_2, the relative phase between the two traps. Because the radial symmetry of u increases with increasing ω, the effect of relative phase diminishes in this regime. Lastly, the two rings of rotation divide the unit disk into two regions of equal area. In fact, it can be easily shown using (3.18) that the optimal radii of rotation for N traps are

$$r_j = \sqrt{\frac{j}{N}}\,, \qquad j = 1, \ldots, N\,. \tag{3.21}$$

The results of [21, 32] show that a single Dirichlet ring on which $u = 0$ is best placed at $r = 1/\sqrt{2}$, which divides the unit disk into two equal areas. In [32], this occurred in the $\omega\to\infty$ regime with $\omega \gg \mathcal{O}(\varepsilon^{-1})$ regime. The result (3.21), showing that the equal division of area in fact occurs in the $\mathcal{O}(1) \ll \omega \ll \mathcal{O}(\varepsilon^{-1})$ subregime, is thus unexpected. In Figure 11, with $r_1 = 1/\sqrt{2}$ fixed, we verify the formula (3.19) with full numerical solutions of (3.3) for various r_2. We observe that $\bar{u}$ is minimized very near $r_2 = 1$, consistent with (3.20). The circles (stars) are for $\theta_2 = 0$ ($\theta_2 = \pi$), their similarity showing that the relative phase of the traps has little effect on $\bar{u}$. We also remark that, in contrast to the case of N optimally placed stationary traps, which share a few concentric rings, (3.21) shows that for sufficiently high rotation frequencies, each trap occupies its *own* ring.

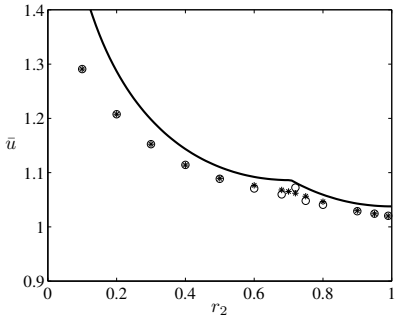

FIG. 11. *Comparison in the regime* $\mathcal{O}(1) \ll \omega \ll \mathcal{O}(\varepsilon^{-1})$ *of* $\bar{u}$ *from* (3.19) *(solid) with that from full numerical solutions of* (3.3) *(circles and stars). One radius of rotation is fixed at* $r_1 = 1/\sqrt{2}$*, while the second* (r_2) *is varied. We observe that* $\bar{u}$ *is minimized very near* $r_2 = 1$*, consistent with* (3.20)*. Here,* $\omega = 500$ *and* $\varepsilon = 1 \times 10^{-4}$*. The circles (stars) are for* $\theta_2 = 0$ *(*$\theta_2 = \pi$*), showing that the relative phase of the traps has little effect on* $\bar{u}$*.*

3.3. The regime $\omega \to \infty$ with $\omega \gg \mathcal{O}(\varepsilon^{-1})$. In this regime the MFPT u is radially symmetric and satisfies

$$u_{rr} + \frac{1}{r}u_r + 1 = 0, \quad u(r_j) = 0 \text{ and } u'(0) = u'(1) = 0\,, \qquad 0 \le r_1, \dots, r_N \le 1\,. \tag{3.22}$$

The solution to (3.22) can be obtained in piecewise fashion. The optimal radii are then found by optimizing $\int_0^1 u(r)rdr$ with respect to N variables $r_1, \dots r_N$.

We now show how this N-dimensional optimization problem can be reduced to a sequence of $N-1$ algebraic equations whose solution yields the optimal radii. We first define two functions: let $r_2 = F(r_1, r_3)$ be the optimal ring location r_2 for the MFPT problem on an annulus with Dirichlet boundary conditions on $r = r_1$ and r_3, and with a ring trap at location $r_2 \in (r_1, r_3)$. That is, let

$$r_2 = F(r_1, r_3) = \underset{r_2 \in (r_1, r_3)}{\text{minarg}} \int_{r_1}^{r_3} u(r)rdr\,, \tag{3.23a}$$

where $u(r)$ solves

$$u_{rr} + \frac{1}{r}u_r + 1 = 0, \quad u(r_1) = u(r_2) = u(r_3) = 0. \tag{3.23b}$$

Similarly, let $r_1 = G(r_2)$ be the optimal location of the ring trap of radius r_1 inside a Dirichlet disk of radius r_2 :

$$r_2 = G(r_2) = \underset{r_1 \in (0, r_2)}{\text{minarg}} \int_0^{r_2} u(r)rdr\,, \tag{3.24a}$$

where $u(r)$ solves

$$u_{rr} + \frac{1}{r}u_r + 1 = 0, \quad u(r_1) = u(r_2) = 0, \quad u'(0) = 0. \tag{3.24b}$$

The following are three key observations that allow us to "decouple" the problem.

- Observation 1. For an optimal configuration $r_1, \dots, r_N$ which minimizes $\min_{r_1,\dots,r_N} \int_0^1 u(r)rdr$ of problem (3.22), one has that $r_1 = G(r_2)$, $r_2 = F(r_1, r_3)$, $\dots, r_{N-1} = F(r_{N-2}, r_N)$. In other words, r_2 is optimal for the MFPT with Dirichlet boundary conditions of an annulus of radii r_1 and r_3, and so on.

- Observation 2. If $r_2 = F(r_1, r_3)$, then $\frac{r_2}{r_3} = F(\frac{r_1}{r_3}, 1)$, and similarly, $r_1 = G(r_2) \iff \frac{r_1}{r_2} = G(1)$. This is a simple consequence of the geometric invariance under the scaling of space.
- Observation 3. Let $A_1, \ldots, A_{N+1}$ be the areas of the regions that are obtained by cutting the disk along the radii $r_1, \ldots, r_N$. Then the sum of even areas is equal to the sum of odd areas. We show below that this condition may be written as

$$r_1^2 - r_2^2 + r_3^2 - \cdots + (-1)^N r_N^2 - (-1)^N \frac{1}{2} = 0. \tag{3.25}$$

The first two observations yield the following algorithm to compute the optimal radii of rotation $r_1, \ldots, r_N$. First, define

$$z_i = \frac{r_i}{r_{i+1}}, \qquad i = 1, \ldots, N-1. \tag{3.26}$$

Then from Observation 2, we have that z_1 satisfies $z_1 = G(1)$, while z_i for $i > 1$ may be found sequentially by solving $z_2 = F(z_1 z_2, 1), \ldots, z_{N-1} = F(z_{N-1} z_N, 1)$. Once we determine $z_1, \ldots, z_{N-1}$, the radii $r_1, \ldots, r_N$ are found by simultaneously solving (3.25) and (3.26).

Explicit solutions of (3.23) and (3.24) show, respectively, that z_1 satisfies

$$4 - \frac{z_1^2 - 1}{z_1^2 \ln(z_1)} = 0\,, \tag{3.27}$$

while z_{i+1} is related to z_i through

$$4 - \frac{z_{i+1}^2 - 1}{z_{i+1}^2 \ln(z_{i+1})} = \frac{z_i^2 - 1}{\ln(z_i)}, \quad i \geq 1. \tag{3.28}$$

Note that the values of z_i are universal and do not depend on N. The first seven values of z_i are approximately

k	1	2	3	4	5	6	7
z_k	0.533543	0.712445	0.792159	0.837265	0.866283	0.886517	0.901433

To illustrate this method, we consider the case of $N = 3$ rings. Then we have

$$r_1 = z_1 z_2 r_3\,, \qquad r_2 = z_2 r_3, \qquad r_3 = \sqrt{\frac{1/2}{(z_1 z_2)^2 - (z_2)^2 + 1}}\,, \tag{3.29}$$

which yields the optimal radii of rotation for the three traps $r_1 = 0.33679, r_2 = 0.63124, r_3 = 0.886022$. We observe that these radii satisfy (3.25) of Observation 3, which we show here. First, consider the following problem:

$$r_m = \underset{r_m \in (r_i, r_o)}{\operatorname{minarg}} \int_{r_i}^{r_o} u(r) r dr\,, \tag{3.30a}$$

where $u(r)$ solves

$$u_{rr} + \frac{1}{r} u_r + 1 = 0, \qquad u'(r_i) = u'(r_o) = 0, \qquad u(r_m) = 0. \tag{3.30b}$$

For a fixed r_m, $u(r)$ is given by

$$u = \begin{cases} \dfrac{r_m^2 - r^2}{4} + \dfrac{r_i^2}{2} \ln\left(r/r_m\right), & r_i < r < r_m; \\ \dfrac{r_m^2 - r^2}{4} + \dfrac{r_o^2}{2} \ln\left(r/r_m\right), & r_m < r < r_o. \end{cases}$$

To find r_m which minimizes (3.30), we compute

$$\frac{\partial}{\partial r_m} \int_{r_i}^{r_o} u(r) r dr = \int_{r_i}^{r_o} \left(\frac{\partial}{\partial r_m} u\right) r dr = \frac{1}{4r_m}\left(r_m^2 - r_i^2\right)^2 - \frac{1}{4r_m}\left(r_m^2 - r_o^2\right)^2 = 0\,.$$

It follows that the minimizing r_m satisfies

$$r_m^2 - r_i^2 = r_o^2 - r_m^2. \tag{3.31}$$

We conclude that for the problem (3.30), the optimal r_m divides the annulus into two regions of equal area. Now consider the optimal solution to (3.22). As an example of this theory, the case $N = 3$ is considered and the optimal solution $u(r)$ shown in Figure 12. The solution $u(r)$ is plotted along with the interior maximizers of u by r_{12} and r_{23} and the areas between maxima and zeros of u as shown. By the property (3.31), we have

$$A_1 = A_{21}, \qquad A_{22} = A_{31}, \qquad A_{32} = A_4\,. \tag{3.32}$$

Moreover, we have

$$A_2 = A_{21} + A_{22}, \qquad A_3 = A_{31} + A_{32}, \tag{3.33}$$

where $A_1, \ldots, A_4$ are the areas of the regions that are obtained by cutting the disk along the radii $r_1, \ldots, r_3$. It follows from (3.32) and (3.33) that $A_1 + A_3 = A_2 + A_4$. This is equivalent to (3.29).

In Figure 13, we compare the optimal radii in this $\omega \to \infty$ with $\omega \gg \mathcal{O}(\varepsilon^{-1})$ regime (top row) against those in the $\mathcal{O}(1) \ll \omega \ll \mathcal{O}(\varepsilon^{-1})$ regime (bottom row). In the top row, we observe that as N increases, the outer rings appear to be equally spaced. By contrast, in the bottom row, the ring locations have an explicit formula $r_i = \sqrt{i/N}$ for $i = 1, \ldots, N$ and tend to concentrate nearer to the boundary.

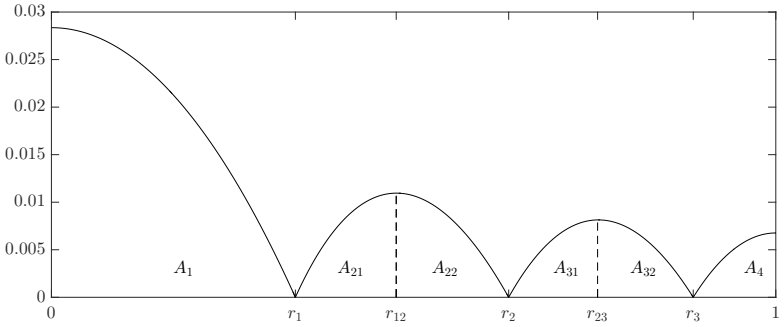

FIG. 12. *Plot of the solution $u(r)$ to (3.22) for $N = 3$ with traps located at the optimal radii.*

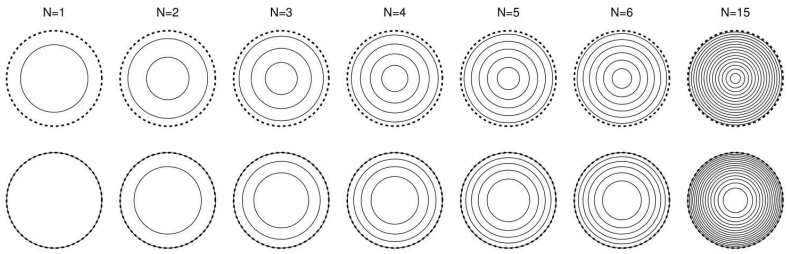

FIG. 13. *Top row: optimal ring positions when* $\omega \gg \mathcal{O}(\varepsilon^{-1})$. *Bottom row: optimal ring positions when* $\mathcal{O}(1) \ll \omega \ll \mathcal{O}(\varepsilon^{-1})$. *The ring locations are indicated by solid lines and the boundary* $r = 1$ *of the disk is denoted by a dashed line. In the bottom row, the outermost ring* r_N *coincides with the boundary.*

3.4. The regime $\omega \sim \mathcal{O}(\varepsilon^{-1})$. The distinguished regime $\omega = \varepsilon^{-1}\omega_0$ with $\omega_0 = \mathcal{O}(1)$ marks the transition between the $1 \ll \omega \ll \mathcal{O}(\varepsilon^{-1})$ regime of section 3.2 and the $\omega \to \infty$ regime with $\omega \gg \mathcal{O}(\varepsilon^{-1})$ analyzed in section 3.3. In this regime, the equation in the $\mathcal{O}(\varepsilon)$ jth inner region is no longer the radially symmetric Laplace's equation outside the unit disk. Indeed, with scaling $\mathbf{y} = \varepsilon^{-1}(\mathbf{x} - \mathbf{x}_j)$, both the Δu and $\omega\partial_\theta u$ terms in (3.3) become $\mathcal{O}(\varepsilon^{-2})$. Recalling that the relative phases of the traps have little effect on $\bar{u}$ in the high frequency regimes, we assume for simplicity that they are all located on $\theta_j = 0$. With $u(\mathbf{x}_j + \varepsilon\mathbf{y}) = U_{j0}(\mathbf{y}) + \mathcal{O}(\sqrt{\varepsilon})$, the leading order equation in the jth inner region then becomes

$$\Delta U_{j0} + \omega_0 r_j \frac{\partial}{\partial y_2} U_{j0} = 0\,, \quad |\mathbf{y}| > 1\,, \quad U_{j0} = 0\,, \quad |\mathbf{y}| = 1\,, \tag{3.34a}$$

$$U_{j0} \sim u_{0j}(\omega_0 r_j) \ \text{ as } \ |\mathbf{y}| \to \infty\,; \qquad \mathbf{y} = (y_1, y_2),$$

where $u_{0j}(\omega_0 r_j)$ is a constant to be found. This inner solution and the outer solution are mediated through an intermediate parabolic layer with scaling $\hat{r} = \sqrt{\omega_0}(r - r_j)/\sqrt{\varepsilon}$ and $\hat{\theta} = 2\pi - \theta$, forming an $\mathcal{O}(\sqrt{\varepsilon})$ layer around the ring $r = r_j$. In this layer, we expand $u = \hat{u}_{j0} + \mathcal{O}(\sqrt{\varepsilon})$ so that at the leading order, we obtain the parabolic equation for $\hat{u}_{j0}$

$$\hat{u}_{j0\hat{r}\hat{r}} - \hat{u}_{j0\hat{\theta}} = 0\,, \qquad \hat{u}_{j0}(\hat{r}, 0) = u_{0j} + \mathcal{O}(\sqrt{\varepsilon})\,, \qquad \hat{u}_{j0} \sim \text{constant as } \hat{r} \to \pm\infty\,, \tag{3.34b}$$

where u_{0j} is an $\mathcal{O}(1)$ constant. The solution of (3.34b) is simply $\hat{u}_{j0} = u_{0j}$ so that u in the outer region is approximately constant on the ring $r = r_j$.

In the outer region, we expand the solution as $u = u_0 + \sqrt{\varepsilon}u_1$. Substituting this expansion into (3.3) with $\omega = \varepsilon^{-1}\omega_0$, we obtain at $\mathcal{O}(\varepsilon^{-1})$ and $\mathcal{O}(\varepsilon^{-1/2})$ that $u_{0\theta} = u_{1\theta} = 0$. That is, the outer solution is radially symmetric to $\mathcal{O}(\sqrt{\varepsilon})$. At $\mathcal{O}(1)$ with $u_{0\theta} = 0$, we obtain the radially symmetric ODE for u_0

$$u_{0rr} + \frac{1}{r}u_{0r} + 1 = 0\,, \qquad u_0 = u_{0j}\,, \quad r = r_j\,, \qquad u_0'(0) = u_0'(1) = 0\,, \tag{3.34c}$$

where the constants u_{0j} are to be found by matching fluxes in the outer and elliptic regions. The solution to (3.34) was found in [32] for a single rotating trap using a hybrid asymptotic-numerical technique similar to that employed in [9]. Here, we extend the method to the case of two traps, noting that extension to N traps follows in

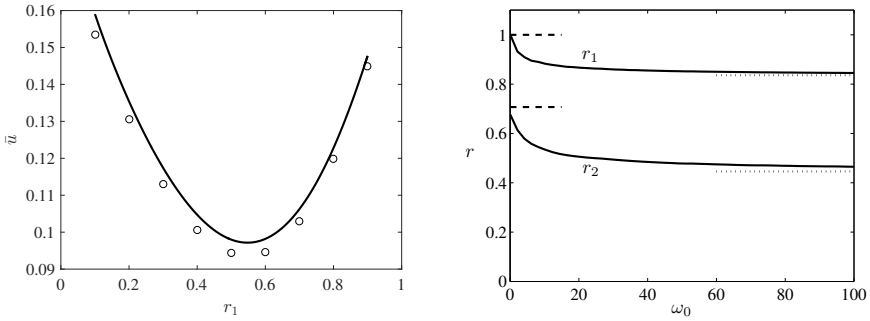

(a) $\bar{u}$ versus r_1. (b) Optimal radii of rotation.

FIG. 14. *In* (a)*, with* $\omega_0 = 10$*,* $\varepsilon = 0.001$*, and* $r_2 = 0.95$*, we compare* $\bar{u}$ *in* (3.36) *for a range of* r_1 *(solid) against full numerical results of* (3.3) *(circles). The asymptotic result* (3.36) *correctly predicts the location of the minimum. In* (b)*, we show optimal radii* r_1 *and* r_2 *that minimize* $\bar{u}$*. The dashed lines are the optimal radii* $r_1 = 1/\sqrt{2}$ *and* $r_2 = 1$ *in the limit* $\omega_0 \to 0$*. The dotted lines represent the limit in which* $\omega_0 \to \infty$*, discussed in section* 3.3.

the same manner. Using a hybrid asymptotic-numerical method detailed in Appendix A, we calculate that u_{01} and u_{02} are given by

(3.35)
$$u_{01} = \frac{1}{2}\frac{u_{c1}\left(r_1^2 - r_2^2 - 4u_{c2}\right)}{2\log\frac{r_1}{r_2} - 2u_{c1} - 2u_{c2}}, \qquad u_{02} = \frac{1}{2}\frac{u_{c2}\left(2\log\frac{r_1}{r_2} - r_1^2 + r_2^2 - 4u_{c1}\right)}{\log\frac{r_1}{r_2} - 2u_{c1} - 2u_{c2}}, \quad r_1 < r_2,$$

where the constants u_{c1} and u_{c2} are obtained numerically from a canonical elliptic problem. The mean of u is then obtained from computing the mean of the solution of (3.34c), which yields

(3.36)
$$\bar{u} = \frac{1}{8\log\frac{r_1}{r_2}}\left[\left(r_2^2 - r_1^2\right)\left(r_2^2 - r_1^2 + 4(u_{02} - u_{01})\right) + \left(4r_2^2 + 8u_{02} - 3 - 4\log r_2\right)\log\frac{r_1}{r_2}\right] + \mathcal{O}(\sqrt{\varepsilon}), \qquad r_1 < r_2\,.$$

In Figure 14(a), with $\omega_0 = 10$, $\varepsilon = 0.001$, and $r_2 = 0.95$, we compare (3.36) (solid) with full numerical solutions of (3.3) (circles) for a range of r_1. We observe good agreement not only in the value of $\bar{u}$, but in where the minimum occurs. Further confirmation of the analysis (not shown) comes from the agreement of u_{01} and u_{02} given asymptotically by (3.35) with that obtained from numerical solutions of (3.3). In Figure 14(b), we show the optimal radii of rotation obtained from optimizing (3.36) with respect to r_1 and r_2.

We recall that this regime interpolates between the results of the $\mathcal{O}(1) \ll \omega \ll \mathcal{O}(\varepsilon^{-1})$ subregime ($\omega_0 \to 0$) and the $\omega \to \infty$ regime with $\omega \gg \mathcal{O}(\varepsilon^{-1})$ ($\omega_0 \to \infty$). Indeed, taking the latter limit in (3.34a), it is simple to see that since $\partial_{y_2} U_j = 0$ and $U_j = 0$ on $\partial\Omega_0$, we must have $u_j = 0$. This corresponds to the case in which $u = 0$ on the ring $r = r_j$, which occurs in the limit of infinitely fast trap rotation. This limit was discussed in detail in section 3.3, the two-trap result of which is represented by the dotted lines in Figure 14(b). Analysis of the former limit $\omega_0 \to 0$ (dashed lines in Figure 14(b)) in Appendix A shows that the transition between the optimal configurations of the regimes $\mathcal{O}(1) \ll \omega \ll \mathcal{O}(\varepsilon^{-1})$ and $\omega \sim \mathcal{O}(\varepsilon^{-1})$ is smooth.

We make as a final remark that to calculate the $\mathcal{O}(\sqrt{\varepsilon})$ correction to (3.36), we must calculate the solution of the $\mathcal{O}(\sqrt{\varepsilon})$ outer problem

$$u_{1rr} + \frac{1}{r}u_{1r} = 0\,, \qquad u_1 = u_{1j}\,, \quad r = r_j\,, \qquad u_1'(0) = u_1'(1) = 0\,. \tag{3.37}$$

The constants u_{1j} in (3.37) uniquely determine u_1 and may be calculated by employing a higher order matching between the three regions. In particular, the far-field conditions of the elliptic layer must be matched to the "initial conditions" of the parabolic layer, while the far-field conditions of the parabolic layer must be matched to the local gradient of u_0 near $r = r_j$. By imposing periodicity in the parabolic layer along with a higher order matching between the parabolic and elliptic layers, a certain terminal value problem can be formulated for which a numerical solution yields u_{1j}. This is a lengthy analysis that we omit for brevity.

4. Discussion. We have used the techniques from [21, 33, 32] to study the MFPT in the presence of multiple mobile traps in one and two dimensions. Very surprising and intricate behavior is observed even in a one-dimensional setting, where we find an infinite sequence of bifurcations (two oscillating traps switch from an in-phase to an antiphase configuration infinitely many times) as the oscillation frequency ω is increased. When a trap is forced to adapt to two neighbors whose dynamics are predetermined, its optimal strategy may be neither in phase nor antiphase with either neighbor.

In two dimensions, the presence of multiple distinguished regimes allows for the characterization of distinct optimal configurations. The simplest of these regimes is $\omega \gg \mathcal{O}(\varepsilon^{-1})$, in which case each rotating trap becomes a Dirichlet ring inside a disk. It is interesting to contrast this to the regime $\mathcal{O}(1) \ll \omega \ll \mathcal{O}(\varepsilon^{-1})$, for which each trap becomes a "ring" but instead of a pure Dirichlet condition on a ring, it is more "porous," yielding different optimal radii. For both of these regimes, the relative phase between the two traps is insignificant to leading order, and it is an open question to find the optimal phase. In the $\omega \sim \mathcal{O}(1)$ regime, we observe a bifurcation in which the optimal configuration changes from antiphase rotation with a common radius to an in-phase rotation on well-separated rings.

While our analysis of all regimes is valid for three or more traps, the complexity of the numerical optimizations quickly increases with the number of traps. However, we expect that some behavior observed in the two-trap scenario would extend to the $N > 2$ case. For example, if three traps rotate slowly, we expect that they rotate with the same radius separated by a $2\pi/3$ phase and that a similar bifurcation occurs as the rotation rate increases. On the other hand it is unclear what resulting phase difference (if any) will result on the other side of the bifurcation. For seven or more traps, where the optimal stationary configuration may be a ring of six traps with one at the origin [21], the bifurcation may be more complex.

Our analysis of the two-dimensional problem was greatly simplified by the rotational symmetry. It would be very interesting to solve (3.2) either numerically or asymptotically to understand the effects on MFPT of more general trap motion. Within the same rotational framework, one could use (3.2) to investigate whether it is more optimal for two traps to rotate in the same or the opposite direction and whether the result depends on rotation rate in a way similar to what was found in section 2 for one dimension.

Another open question is to determine an "optimal" path of the trap. Here, the key issue is to find the right "constraint" on the type of admissible motion. This problem may require an energy constraint, as otherwise one can allow the trap to

travel with infinite speed on a space-filling curve. Whether an energy constraint leads to a well-posed optimization problem and whether other or additional constraints may be more appropriate are interesting modeling questions.

The question of proper constraints also arises in the analogous one-dimensional problem, where one seeks an optimal periodic path of $\mathcal{O}(1)$ amplitude. The problem (2.2) for the MFPT would need to be solved numerically for an arbitrary periodic path expressed in terms of Fourier coefficients, which would then be optimized subject to constraints. For example, one may require a fixed energy output over one period while also penalizing mean square displacement from a certain fixed point.

An overarching theme of this work has been to investigate configurations that result from multiple mobile traps cooperating to optimize a global quantity. It may be interesting to ask what happens when each trap adjusts its motion locally in order to increase its own rate of capturing the Brownian particles and whether this algorithm leads to any stable configurations.

Appendix A. Analysis of the $\boldsymbol{\omega \sim \mathcal{O}(\varepsilon^{-1})}$ regime. We demonstrate here how to compute the quantity u_{0j} in (3.34c). We begin by letting $U_{j0} = u_{0j}(\mu_j + 1)$. Substituting into (3.34a), we obtain for μ_j

(A.1)
$$\Delta\mu_j + q_j \frac{\partial \mu_j}{\partial y_2} = 0\,,\ |\mathbf{y}| > 1\,,\ \mu_j = -1\,,\ |\mathbf{y}| = 1\,,\quad \mu_j \sim 0 \ \text{ as } \ |\mathbf{y}| \to \infty\,;\quad q_j \equiv \omega_0 r_j\,.$$

The quantity we seek is the flux of μ_j on the boundary of the unit disk Ω_0,

$$\Phi_j \equiv \int_{\partial\Omega_0} \frac{\partial \mu_j}{\partial n}\, dS\,, \tag{A.2}$$

where $\partial/\partial n$ denotes the outward normal derivative on $\partial\Omega_0$. The flux may be extracted numerically as follows [32, 9]. We first consider the adjoint Green's function satisfying

$$\Delta\tilde{G} - q_j \frac{\partial \tilde{G}}{\partial \xi_2} = \delta(\boldsymbol{\xi} - \mathbf{z})\,, \qquad \tilde{G} \to 0 \ \text{ as } \ |\boldsymbol{\xi}| \to \infty\,, \tag{A.3}$$

which may be solved to give

$$\tilde{G}(\boldsymbol{\xi};\mathbf{z}) = -\frac{1}{2\pi} e^{\frac{q_j}{2}(\eta - z_2)} K_0\left(\frac{q_j}{2}|\boldsymbol{\xi} - \mathbf{z}|\right)\,; \qquad \boldsymbol{\xi} = (\xi_1, \xi_2)\,,\quad \mathbf{z} = (z_1, z_2)\,. \tag{A.4}$$

In polar coordinates $(\xi_1, \xi_2) \to (\tilde{r}\cos\tilde{\theta}, \tilde{r}\sin\tilde{\theta})$ and $(z_1, z_2) \to (\rho\cos\phi, \rho\sin\phi)$, the solution to (A.1) can then be expressed in terms of $\tilde{G}$ in (A.4) as

(A.5)
$$\mu_j(\rho\cos\phi, \rho\sin\phi) = \int_0^{2\pi} \frac{\partial \tilde{G}}{\partial \tilde{r}}\bigg|_{\tilde{r}=1} d\tilde{\theta} + \int_0^{2\pi} \left(\tilde{G}\,\frac{\partial \mu_j}{\partial \tilde{r}}\right)_{\tilde{r}=1} d\tilde{\theta} - q_j \int_0^{2\pi} \tilde{G}\bigg|_{\tilde{r}=1} \sin\tilde{\theta}\, d\tilde{\theta}\,.$$

Note that all integrals in (A.5) are over the boundary of the unit disk $\partial\Omega_0$. To extract the flux $\partial\mu_j/\partial\tilde{r}|_{\tilde{r}=1}$, we impose the boundary condition $\mu_j = -1$ on $\rho = 1$, yielding

$$-\int_0^{2\pi} \tilde{G}\bigg|_{\tilde{r}=\rho=1} \frac{\partial \mu_j}{\partial \tilde{r}}\bigg|_{\tilde{r}=1} d\tilde{\theta} = \frac{1}{2} + \int_0^{2\pi} \frac{\partial \tilde{G}}{\partial \tilde{r}} - s_0 \tilde{G}\sin\tilde{\theta}\bigg|_{\tilde{r}=\rho=1} d\tilde{\theta}\,. \tag{A.6}$$

In (A.6), the $1/2$ term is a result of evaluating μ_j on $\partial\Omega_0$ and thus integrating over only half of the delta function in its Green's function representation. The second

term may be computed from integrating by parts the equation for the adjoint Green's function (A.3) over $|\boldsymbol{\xi}| > 1$, which finally yields

$$\int_0^{2\pi} \tilde{G}\left|_{\tilde{r}=\rho=1} \frac{\partial \mu_j}{\partial \tilde{r}}\right|_{\tilde{r}=1} d\tilde{\theta} = -1\,. \tag{A.7}$$

The integral equation (A.7) may then be solved numerically for $\partial\mu_j/\partial\tilde{r}|_{\tilde{r}=1}$ by expressing the latter as a Fourier series and solving a system of equations for the coefficients.

To express Φ_j in terms of the flux f_j of u_0, we recall that $u_0 \sim u_{0j}(\mu_j + 1)$ near $\mathbf{x} = \mathbf{x}_j$. Substituting into (A.2), we obtain

$$u_{0j} = \frac{f_j}{\int_{\partial\Omega_0} \frac{\partial \mu_j}{\partial n}\, dS} = -\frac{f_j}{\pi} \frac{-\pi}{\int_{\partial\Omega_0} \frac{\partial \mu_j}{\partial n}\, dS}\,, \tag{A.8}$$

where f_j is the flux of u on the jth trap. We rewrite (A.8) as

$$u_{0j} = -\frac{f_j}{\pi} u_{cj}\,, \qquad u_{cj} \equiv \frac{-\pi}{\Phi_j}, \tag{A.9}$$

where Φ_j is defined in (A.2). The quantity $u_{cj}(q_j)$, whose dependence on $q_j \equiv \omega_0 r_j$ is through that of μ_j, was computed in [32] and reproduced in Figure 15. To find u_{0j} in (A.9), we require N equations for f_j. We demonstrate this for two traps. In the three distinct regions, we compute u_r as

$$u_r = -\frac{r}{2} + \begin{cases} 0, & 0 < r < r_1; \\ \dfrac{c}{r}, & r_1 < r < r_2; \\ \frac{1}{2r}, & r_2 < r < 1, \end{cases} \qquad c \equiv \frac{1}{\log \frac{r_1}{r_2}} \left[u_{01} - u_{02} + \frac{1}{4}\left(r_1^2 - r_2^2\right)\right]. \tag{A.10}$$

The total fluxes on the rings $r = r_1$ and $r = r_2$ must, respectively, be f_1 and f_2. We calculate that

$$f_1 = -2\pi c\,, \qquad f_2 = 2\pi c - \pi\,. \tag{A.11}$$

We remark that $f_1 + f_2 = -\pi$, as expected from applying the divergence theorem to (3.3). Finally, with c defined in (A.10), we obtain u_{01} and u_{02} as given in (3.35).

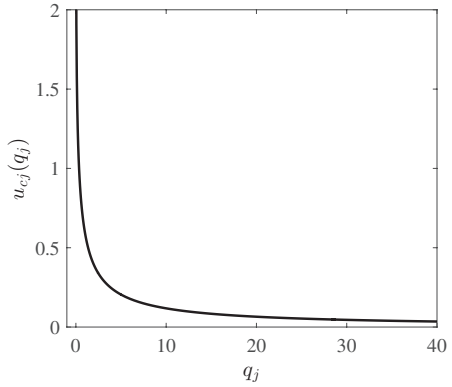

FIG. 15. *Plot of u_{cj} versus $q_j \equiv \omega_0 r_j$.*

To analyze the limit $\omega_0 \to 0$ (dashed lines in Figure 14(b)), we must look at the corresponding limit $q_j \to 0$ in (A.4) and (A.7). From the asymptotics of modified Bessel functions, we calculate the leading order behavior of $\tilde{G}$ and $\partial_{\tilde{r}}\tilde{G}|_{\tilde{r}=\rho=1}$

$$\tilde{G} \sim \frac{1}{2\pi}\left[\log q_j + \log|\boldsymbol{\xi}-\mathbf{z}| - \log 4 + \gamma\right] + \mathcal{O}(q_j \log q_j)\,,$$
$$\left.\frac{\partial \tilde{G}}{\partial \tilde{r}}\right|_{\tilde{r}=\rho=1} \sim \frac{1}{4\pi} + \mathcal{O}(q_j) \qquad \text{as } \; q_j \to 0\,, \tag{A.12}$$

where γ is Euler's constant. With (A.12) in (A.7), we have to leading order that

$$-\frac{1}{2\pi}\left[\log q_j - \log 4 + \gamma\right] \times \int_0^{2\pi} \left.\frac{\partial \mu_j}{\partial \tilde{r}}\right|_{\tilde{r}=1} d\tilde{\theta} - \frac{1}{4\pi}\int_0^{2\pi} \log\Big[(\cos\tilde{\theta}-\cos\phi)^2 + (\sin\tilde{\theta}-\sin\phi)^2\Big] \left.\frac{\partial \mu_j}{\partial \tilde{r}}\right|_{\tilde{r}=1} d\tilde{\theta} = 1. \tag{A.13}$$

Since the limit $\omega_0 \to 0$ in (A.1) corresponds to μ_j approaching a radially symmetric solution, we assume that $\partial_{\tilde{r}}\mu_j$ is uniform on $\partial\Omega_0$. The second term in (A.13) consequently integrates to zero, leaving

$$\int_0^{2\pi} \left.\frac{\partial \mu_j}{\partial \tilde{r}}\right|_{\tilde{r}=1} d\tilde{\theta} \sim -\frac{2\pi}{\log q_j - \log 4 + \gamma}\,. \tag{A.14}$$

Using (A.14) in (A.9), and noting that $\partial_n = -\partial_{\tilde{r}}$, we obtain the asymptotic behavior of u_{cj} in the limit of small q_j

$$u_{cj} \sim -\frac{1}{2}\left[\log q_j - \log 4 + \gamma\right]\,. \tag{A.15}$$

With $q_j = \omega_0 r_j$, substituting (A.15) for u_{c1} and u_{c2} into (3.36) and discarding terms of $\mathcal{O}(1/\log\omega_0)$ results in precisely (3.19). The optimal radii of rotation then, as depicted in Figure 14(b), approach $r_1 = 1/\sqrt{2}$ and $r_2 = 1$ (dashed lines) as $\omega_0 \to 0$. As such, the transition between the results of the regimes $\mathcal{O}(1) \ll \omega \ll \mathcal{O}(\varepsilon^{-1})$ and $\omega \sim \mathcal{O}(\varepsilon^{-1})$ is smooth.

Acknowledgments. We gratefully acknowledge the anonymous reviewers whose feedback improved the presentation of this article.

REFERENCES

[1] *FlexPDE*, www.pdesolutions.com.
[2] O. Bénichou and R. Voituriez, *Narrow-escape time problem: Time needed for a particle to exit a confining domain through a small window*, Physical Rev. Lett., 100 (2008), pp. 168–105.
[3] O. Bénichou and R. Voituriez, *From first-passage times of random walks in confinement to geometry-controlled kinetics*, Phys. Rep., 539 (2014), pp. 225–284.
[4] A. J. Bray and R. A. Blythe, *Exact asymptotics for one-dimensional diffusion with mobile traps*, Physical Rev. Lett., 89 (2002), pp. 150–601.
[5] A. J. Bray and R. Smith, *The survival probability of a diffusing particle constrained by two moving, absorbing boundaries*, J. Phys. A, 40 (2007), F235.
[6] P. C. Bressloff and S. D. Lawley, *Escape from subcellular domains with randomly switching boundaries*, Multiscale Model. Simul., 13 (2015), pp. 1420–1445.
[7] P. C. Bressloff and J. M. Newby, *Stochastic models of intracellular transport*, Rev. Modern Phys., 85 (2013), 135.

[8] A. F. Cheviakov, M. J. Ward, and R. Straube, *An asymptotic analysis of the mean first passage time for narrow escape problems: Part* II: *The sphere*, Multiscale Model. Simul., 8 (2010), pp. 836–870.

[9] J. Choi, D. Margetis, T. M. Squires, and M. Z. Bazant, *Steady advection–diffusion around finite absorbers in two-dimensional potential flows*, J. Fluid Mech., 536 (2005), pp. 155–184.

[10] M. Chupeau, O. Bénichou, and S. Redner, *Optimal Strategy to Capture a Skittish Lamb Wandering Near a Precipice*, preprint, arXiv:1504.05107, 2015.

[11] D. A. Darling and A. Siegert, *The first passage problem for a continuous Markov process*, Ann. Math. Statist., 24 (1953), pp. 624–639.

[12] M. I. Delgado, M. J. Ward, and D. Coombs, *Conditional mean first passage times to small traps in a 3-D domain with a sticky boundary: Applications to T cell searching behaviour in lymph nodes*, Multiscale Model. Simul., 13 (2015), pp. 1224–1258.

[13] C. Dingwall and R. A. Laskey, *Protein import into the cell nucleus*, Ann. Rev. Cell Biol., 2 (1986), pp. 367–390.

[14] C. M. Feldherr, E. Kallenbach, and N. Schultz, *Movement of a karyophilic protein through the nuclear pores of oocytes*, J. Cell Biol., 99 (1984), pp. 2216–2222.

[15] L. Giuggioli, S. Pérez-Becker, and D. P. Sanders, *Encounter times in overlapping domains: Application to epidemic spread in a population of territorial animals*, Phys. Rev. Lett., 110 (2013), pp. 58–103.

[16] D. Görlich and U. Kutay, *Transport between the cell nucleus and the cytoplasm*, Ann. Rev. Cell Developmental Biology, 15 (1999), pp. 607–660.

[17] D. Holcman and I. Kupka, *The probability of an encounter of two Brownian particles before escape*, J. Phys. A, 42 (2009), pp. 315–210.

[18] D. Holcman and Z. Schuss, *Escape through a small opening: receptor trafficking in a synaptic membrane*, J. Stat. Phys., 117 (2004), pp. 975–1014.

[19] D. Holcman and Z. Schuss, *The narrow escape problem*, SIAM Rev., 56 (2014), pp. 213–257.

[20] D. Holcman and Z. Schuss, *Stochastic Narrow Escape in Molecular and Cellular Biology: Analysis and Applications*. Springer, New York, 2015.

[21] T. Kolokolnikov, M. S. Titcombe, and M. J. Ward, *Optimizing the fundamental Neumann eigenvalue for the Laplacian in a domain with small traps*, European J. Appl. Math., 16 (2005), pp. 161–200.

[22] A. E. Lindsay, T. Kolokolnikov, and J. C. Tzou, *Narrow escape problem with a mixed trap and the effect of orientation*, Phys. Rev. E, 91 (2015), pp. 32–111.

[23] S. Pillay, M. J. Ward, A. Peirce, and T. Kolokolnikov, *An asymptotic analysis of the mean first passage time for narrow escape problems: Part* I: *Two-dimensional domains*, Multiscale Model. Simul., 8 (2010), pp. 803–835.

[24] T. Ransford, *Potential Theory in the Complex Plane*, London Math. Soc. Stud. Texts 28. Cambridge University Press, Cambridge, UK, 1995.

[25] S. Redner, *A Guide to First-Passage Processes*. Cambridge University Press, Cambridge, UK, 2001.

[26] Z. Schuss, A. Singer, and D. Holcman, *The narrow escape problem for diffusion in cellular microdomains*, Proc. Nat. Acad. Sci. USA, 104 (2007), pp. 16098–16103.

[27] A. Singer, Z. Schuss, D. Holcman, and R. S. Eisenberg, *Narrow escape, Part* I, J. Stat. Phys., 122 (2006), pp. 437–463.

[28] A. Singer, Z. Schuss, and D. Holcman, *Narrow escape, Part* II: *The circular disk*, J. Stat. Phys., 122 (2006), pp. 465–489.

[29] P. J. Strzyz, H. O. Lee, J. Sidhaye, I. P. Weber, L. C. Leung, and C. Norden, *Interkinetic nuclear migration is centrosome independent and ensures apical cell division to maintain tissue integrity*, Developmental Cell, 32 (2015), pp. 203–219.

[30] V. Tejedor, O. Bénichou, R. Metzler, and R. Voituriez, *Residual mean first-passage time for jump processes: Theory and applications to Lévy flights and fractional Brownian motion*, J. Phys. A, 44 (2011), pp. 255–003.

[31] H. C. Tuckwell and F. Y. M. Wan, *First-passage time of Markov process to moving barriers*, J. Appl. Probab., 21 (1984), pp. 695–709.

[32] J. C. Tzou and T. Kolokolnikov, *Mean first passage time for a small rotating trap inside a reflective disk*, Multiscale Model. Simul., 13 (2015), pp. 231–255.

[33] J. C. Tzou, S. Xie, and T. Kolokolnikov, *First-passage times, mobile traps, and Hopf bifurcations*, Phys. Rev. E, 90 (2014), pp. 62–138.